Naval Research Laboratory

Monterey, CA 93943-5502

Preliminary Evaluation of the Impacts of Aerosol Particles on Laser Performance in the Coastal Marine Boundary Layer

JEFFREY S. REID
DOUGLAS L. WESTPHAL

Atmospheric Dynamics and Prediction Branch
Marine Meteorology Divison

RICHARD M. PAULUS

SPAWAR Systems Center, San Diego
Atmospheric Propagation Branch

SI-CHEE TSAY

NASA Goddard SFC
Climate and Radiation Branch

ALEXANDER VAN EIJK

TNO Netherlands

June 21, 2004

20040903 094

REPORT DOCUMENTATION PAGE

Form Approved
OMB No. 0704-0188

1. REPORT DATE (DD-MM-YYYY)	2. REPORT TYPE	3. DATES COVERED (From - To)
11 June 2004	Memorandum Report	January 4, 2002-January 7, 2003

4. TITLE AND SUBTITLE

Preliminary Evaluation of the Impacts of Aerosol Particles on Laser Performance in the Coastal Marine Boundary Layer

5a. CONTRACT NUMBER
N0001402WX20261AA to SSC-SD

5b. GRANT NUMBER

5c. PROGRAM ELEMENT NUMBER

6. AUTHOR(S)

Jeffrey S. Reid, Douglas L. Westphal, Richard M. Paulus,* Si-Chee Tsay,† and Alexander van Eijk‡

5d. PROJECT NUMBER

5e. TASK NUMBER

5f. WORK UNIT NUMBER

7. PERFORMING ORGANIZATION NAME(S) AND ADDRESS(ES)

Naval Research Laboratory, Code 7534
J.S. Reid and D.L. Westphal
7 Grace Hopper Street, Stop 2
Monterey, CA 93043-5502

8. PERFORMING ORGANIZATION REPORT NUMBER

NRL/MR/7534--04-8803

9. SPONSORING / MONITORING AGENCY NAME(S) AND ADDRESS(ES)

Office of Naval Research, Code 35
Dr. Gil Graf
800 North Quincy Street
Arlington, VA 22217-5660

Office of Naval Research, Code 32
Dr. Ronald Ferek
800 North Quincy Street
Arlington, VA 22217-5660

10. SPONSOR / MONITOR'S ACRONYM(S)

11. SPONSOR / MONITOR'S REPORT NUMBER(S)

12. DISTRIBUTION / AVAILABILITY STATEMENT

Approved for public release; distribution is unlimited.

13. SUPPLEMENTARY NOTES

*Atmospheric Propagation Branch, SPAWAR Systems Center, San Diego ‡TNO Netherlands †NASA Goddard SFC, Climate and Radiation Branch

14. ABSTRACT

This report summarized work performed by the Naval Research Laboratory, SPAWAR Systems Center-San Diego, NASA GSFC and TNO Netherlands on preliminary assessments of the impact of aerosol particles on High Energy Laser performance. While there is only fair visibility in many sensitive parts of the globe, including the Persian Gulf/Arabian Sea, East Asia, and some parts of the Mediterranean Sea, extremely poor visibility events are more rare and are unlikely to be catastrophic to a HEL system. Along coastal regions, dust, pollution, and smoke can be present, which will impair performance over long path lengths. Sea salt and haze can also be significant in regions with considerable stratus cloud cover (such as parts of East Asia and the Arabian Sea). While wavelength optimization is straightforward with respect to water vapor, atmospheric dust, and sea salt, the presence of urban pollution and smoke can complicate the analysis and an optimum wavelength becomes site specific.

15. SUBJECT TERMS

Visibility; Coastal environment; Laser propagation; Meteorology; Aerosol; Climatology

16. SECURITY CLASSIFICATION OF:			17. LIMITATION OF ABSTRACT	18. NUMBER OF PAGES	19a. NAME OF RESPONSIBLE PERSON
a. REPORT	b. ABSTRACT	c. THIS PAGE	UL	63	Jeffrey S. Reid
Unclassified	Unclassified	Unclassified			19b. TELEPHONE NUMBER (include area code) (831) 656-4763

Standard Form 298 (Rev. 8-98)
Prescribed by ANSI Std. Z39.18

CONTENTS

PRELIMINARY EVALUATION OF THE IMPACTS OF AEROSOL PARTICLES ON LASER PERFORMANCE IN THE COASTAL MARINE BOUNDARY LAYER

1. EXECUTIVE SUMMARY

To date, there does not exist a coastal aerosol climatology suitable for electro-optical (EO) systems engineering or planning purposes. In FY2002 a program was initiated by the Office of Naval Research (ONR) Code 351 to develop and extend existing aerosol data into products usable to the High Energy Laser (HEL) engineering community. This work drew heavily on work being conducted by ONR Code 322. The ultimate goal was to transition a global visibility/EO aerosol extinction model and climatology for the purpose of determining aerosol light-scattering impacts on the performance of near-infrared systems such as HEL. The principal database for compiling this climatology would be composed of a set of community aerosol data sets, meteorological observations, remote sensing, and numerical model runs. Aerosol microphysics models for anthropogenic pollutants, smoke, dust and sea salt needed to be compiled. Further parameterizations to extend measurements made in the visible spectrum to the IR would be completed. This report describes our findings with respect to the first year's proposed efforts and how they relate to the project's final objectives on estimated propagation loss and optimal wavelength selection. It is written for project management or systems engineers with only limited exposure to the atmospheric sciences.

The specific effects of aerosol particles on HEL propagation in the marine boundary layer is outside of the scope of this study, as it will strongly depend on the nature of the HEL system deployed. Hence we focus on aerosol scattering and absorption issues of relevance to all EO systems operating in the near IR. Overall, the nature of aerosol particle extinction and absorption in the marine environment is highly variable throughout the world. While there is only fair visibility in many sensitive parts of the globe, including the Persian Gulf/Arabian Sea, East Asia, and some parts of the Mediterranean Sea, extremely poor visibility events are more rare. Along coastal regions, dust, pollution and smoke can be present. Sea salt and haze can also be significant in regions with considerable stratus cloud cover (such as parts of East Asia and the Arabian sea). While wavelength optimization is straightforward with respect to water vapor, atmospheric dust and sea salt, the presence of urban pollution and smoke can complicate the analysis. At wavelengths such as 1.06, 1.25, and 1.65 μm, there are periods when absorption by these fine particles may be greater than that of water vapor. Consequently, there is an offsetting effect of fine mode particles and water vapor that gives wavelengths as long as 1.65 μm more favor. Finally, preliminary modeling studies are encouraging. With further analysis, a first order HEL propagation assessment could be obtained with only two or three more years work.

2. HEL PROJECT INTRODUCTION AND RATIONALE

Visibility degradation due to airborne dust, sea salt/haze, smoke, and other pollutants regularly hampers EO system performance in visible and IR wavelengths. To successfully predict the actual performance of systems such as FLIR pods, airborne scanners, and laser communication systems, a relation linking atmospheric conditions (meteorology, aerosol loading, etc.) and visibility degradation is needed. At present, the Navy Aerosol Model (NAM) family of codes and LOWTRAN parameterizations

can be used to assess the aerosol concentration and subsequent visibility degradation. These models are currently being incorporated into U.S. Navy meteorological models and propagation codes for forecasting the impact of the atmosphere on Navy operations and EO systems. Visibility reducing smoke, haze and dust events can occur locally, but are frequently the result of transport from sources hundreds to thousands of kilometers away. In the later case, the current statistically based aerosol models designed for the open ocean (such as the NAM family of codes and LOWTRAN parameterizations) are not valid. Even when validation measurements are made at one location, their applicability to regions several hundred kilometers away is questionable. Existing atmospheric radiation propagation models have difficulty in predicting EO propagation since aerosol particles vary considerably in size, chemistry, and shape. To be useful for system engineering purposes, a visibility model must account for these variances and be capable of modeling long-range transport.

Navy EO prediction systems have historically focused on slant path visibility problems in support of strike warfare (e.g., aircraft to ship). However, recent advances in laser and beam control technology have made systems like the HEL feasible and highlighted the growing need for near-surface laser propagation assessments. Fundamental beam propagation problems for a HEL system are different from airborne surveillance and imaging systems. For one, extinction and absorption for monochromatic light can be calculated without the use of a sophisticated radiative transfer algorithm (unlike wide bandwidth surveillance systems). However, issues relating to viewing geometry, refractivity and turbulence, particle microphysics, and thermal blooming significantly complicate matters.

A significant problem in assessing HEL performance is simply that despite all of the resources available to the Department of Defense (DoD) and the scientific community, sensitive regions of the world are still devoid of data. Climatologies and assessments have been performed in the past (e.g., Goroch and Brown 1980 and Brown and Goroch 1982) but these are outdated and often performed in the wrong context. Climatologies for visible wavelengths are uncertain, and in the near IR accurate assessments simply do not exist. The high degree of variability in meteorology, particle microphysics, and atmospheric transport properties has made what information that does exist more or less qualitative. As an example, visibility-reducing dust events can occur as a result of transport from storms that originate hundreds to thousands of kilometers away. During transport, particles can change in size, and consequently in optical properties. As a result, existing atmospheric radiation propagation models have difficulty in predicting EO propagation when dust and pollutants are a significant factor because of inherent over-simplifications and uncertainties regarding the sources, shapes, composition and vertical distribution of particles. The situation is even more complicated in coastal regions where the atmosphere is never in any form of "steady state"; the current statistically based aerosol models for sea salt and sea spray (such as the NAM family of extinction models) have an uncertainty of an order of magnitude. To be useful for a near surface EO propagation assessment, one must account for variable particle morphology and chemistry over an area larger than the theater of operations, and be capable of modeling long-range transport. Only through such an analysis will we know true uncertainties.

Fortunately, there is a fair amount of data available for a HEL propagation study. The earth science and climate science communities are essentially asking the same questions as the DoD. Fundamentally, both groups are after the same thing - an understanding of distribution of aerosol particles and their subsequent effects on the Earth's radiative properties. It is only the final application of this information, estimating near surface transmittance or climate change that differs. When taken in the context of surface observation, most of the atmospheric science data sets can be applied to HEL needs.

The application of community data sets for our uses is not entirely straightforward; hence the need for this study. For example, global climate data sets tend to emphasize short-wave energy balance, while HEL systems naturally favor the IR (in particular 1.04, 1.06, 1.25, 1.315, 1.625, 2.25, 3.8 and 10.6 μm). In addition, even with the best conditions during well-planned field studies, error bars can be on the order of a factor of two or more. Consequently, data can rarely be taken at face value. Finally, it must be understood that different investigations proceed differently and that all results are not necessarily

comparable. As part of the first year effort in the ONR Code 351 funded project: "Evaluation of the Impacts of Aerosol Particles on High Energy Laser Performance by Using Community Data Sets and a Mesoscale Transport Model," meteorological, aerosol microphysics and remote sensing data was collected and examined. Modifications were also begun on the Coupled Ocean Atmosphere Mesoscale Prediction System (COAMPS^{TM}) to include aerosol particles. Most of the work for this project involves extension and reanalysis of data and products created under programs funded by ONR Code 322.

In this report, we describe our principal findings from our first year of analysis. Observations and findings from the peer-reviewed literature is reviewed and applied to HEL propagation problems. Preliminary data from visibility observations, and satellite aerosol climatologies are used to constrain aerosol microphysical and radiative properties for further HEL modeling studies. Special attention is paid to probable laser wavelengths: 1.04, 1.06, 1.29, 1.315, 1.62, 2.2, 3.8 and 10.6 μm. Near surface sea spray is also discussed. We conclude with a summary of our preliminary findings.

3. FIRST YEAR GOALS AND WORK STATEMENTS

Previous studies of ocean EO propagation have relied on limited statistical regression models. The goal of this project is to improve the assessment of light scattering and absorption by aerosol particles based on available data sets such as surface observations, satellite climatologies, Sun photometer and lidar networks, and large publicly funded field campaigns, and to ultimately estimate aerosol impacts and derive wavelengths of minimal aerosol extinction and absorption. Spectral and spatial gaps in the data set will be modeled using radiative transfer codes and the NRL Aerosol Analysis and Prediction System (NAAPS) in conjunction with COAMPS^{TM}. Near-surface particle modeling (e.g., fluxes) will also be performed by TNO in the Netherlands. In the second and third years of the project, data is to be gathered from a lidar collocated with an existing sun photometer in a sensitive region to provide a short-term, detailed description of the vertical distribution of aerosols. Multi-year climatologies and probabilities of severe propagation impacts in sensitive regions will be developed. The total scatter and absorption coefficient by particles will be assessed at wavelengths 1.04, 1.06, 1.29, 1.315, 1.625, 2.2, 3.8, and 10.6 μm in the Persian Gulf, Straits of Hormuz, Arabian Sea, Sea of Japan, Yellow Sea, South China Sea, Mediterranean, and North Sea. The statistical probability of occurrence distribution will be assessed at 50, 80, 85, 90, and 95%. The scatter coefficient at 20 m above sea level will be evaluated and the vertical profile from 20 to 3000 m will be modeled. These tasks are broken down into six subtasks:

Task 1: *Evaluate HEL performance based on known aerosol microphysical and meteorological properties*

Task 2: *Compile and analyze available surface visibility reports from airports, aircraft, and ships*

Task 3: *Deploy and operate a lidar system in conjunction with a Sun-sky scanning radiometer to characterize the vertical and temporal aerosol climatology of a specific sensitive region of the world*

Task 4: *Generate Applicable Satellite Climatologies*

Task 5: *Near surface Modeling of Laser Propagation*

Task 6: *Extension of COAMPS^{TM} to model multicomponent aerosols.*

Funding for this project was terminated in FY 2003. In this report, we relate our findings and proposed work for the first year. We present preliminary findings on aerosol particles impacts on HEL propagation where appropriate. Our statement of work had all tasks being initiated. Task 1 was to be completed and visibility data for Task 2 were to be compiled. Mean satellite climatology statistics for Task 4 were to be generated. We were to begin compiling SeaCluse model run results for a multitude of environmental conditions for Task 5. Parameterizations of sources, sinks, and transformations of sulfate, smoke, and salt

processes were to begin to be incorporated into COAMPS™ /NAAPS for Task 6. The following sections relate our findings for these specific tasks.

4. AEROSOL PARTICLE MICROPHYSICAL AND RADIATIVE PROPERTIES

The first step in performing a study of the aerosol impacts on HEL systems is to compile existing knowledge on the intensive physical and optical properties of the aerosol particles themselves. Neither of the commonly used aerosol impact models (NAAPS and Target Acquisition Weapons Software (TAWS)) takes advantage of state-of-the-art aerosol microphysics or radiation algorithms. Their visibility models ultimately break down to bulk input variables including mass concentration, humidity, and wind speed. This not only introduces error due to the high degree of environmental uncertainty from local meteorological effects, it also poses a problem when transitioning 6.1-type research products that incorporate more advanced physics and chemistry schemes, since the required input parameters cannot simply be entered. Consequently, simply invoking such schemes as NAAPS would yield little profit for HEL. To fully appreciate the more advanced models for visibility prediction that are required, it is instructive to provide a brief discussion of the properties of the primary aerosol species that will likely effect HEL propagation in the marine boundary layer.

Aerosol particles both scatter and absorb light, the sum of which is termed light extinction. The reduction of monochromatic light intensity due to extinction is given by Beer's Law of Exponential Decay:

$$I = I_o e^{-\tau} = I_o e^{-x b_{ext}} = I_o e^{-x\left(b_{scat} + b_{abs}\right)}$$

where I_o is the initial light intensity at the source, I is the intensity at some distance x, and b_{ext} is defined as the extinction coefficient (in units of m^{-1} or km^{-1}). The extinction coefficient is simply the per unit length sum of the total particle physical cross-sections times some efficiency, Q_{ext}:

$$b_{ext} = \int_o^\infty Q_{ext}\left(d_p, \lambda\right) N(d_p)\left(\frac{\pi}{4}\right) d_p^2 \, dd_p$$

where $N(d_p)$ in the number of particles at size d_p. The efficiency with which a particle can extinguish light is dependent on particle size and wavelength, and may be calculated by using Mie theory. When the particle size distribution is also known, the extinction coefficient can be evaluated.

The product of x and b_{ext} is termed the optical depth τ. An optical depth of 1 implies a 1/e loss of intensity, or ~63%. Physically, the distance at which the optical depth reaches 1 is the mean distance photons will travel without interactions (mean free path). As a rule of thumb, the human eye loses track of an object (e.g, visibility) at an optical depth of 3 to 4. Aerosol extinction processes are termed "linear" processes by the HEL community since there are relatively few absorption lines and the total light extinction coefficient for particles is simply the sum of the scattering and absorption terms, b_{scat} and b_{abs}, which are defined similarly to b_{ext}. Water vapor can be taken into account by simply adding b_s and b_a terms, the per unit length sum of the gas molecule scattering and absorption cross-sections. However, for the purposes of HEL propagation, scattering by gas molecules is typically ignored.

The impact of a given light scattering and absorption coefficient to EO propagation is obviously dependent on a particular systems' configuration, as well as on three "nonlinear" effects. First, gradients in the atmospheric temperature (and to a lesser degree pressure and humidity) above the ocean surface result in a gradient in atmospheric density and refractive index. Consequently, the distance to the horizon

(or the maximum distance some target can be viewed) changes over the ocean as a function of the air-sea temperature difference (ASTD). As is discussed in later sections, in typical coastal conditions, the horizon as viewed at 10 m above ground level can vary between 5 and 10 (or more) km around the geometric horizon of 12 km (i.e., without refractive effects). The stronger the gradient, the stronger the departure from the "geometric" horizon, with more negative ASTDs implying shorter horizons and vice versa. Periods with decreased and increased horizon distances correspond to subrefractive and super-refractive conditions. If bulk refractivity prohibits the viewing of a target at 5 km from a ship, the EO system can tolerate a fairly high degree of aerosol scattering. Conversely, under super-refractive conditions when light rays are bent over the horizon, aerosol extinction becomes more important if the EO system wishes to take advantage of this excess range.

Second, on a much shorter spatial and temporal scale, turbulence and the exchange of heat between the ocean surface and the atmosphere create variations in the atmosphere's refractive index. As this variation is more chaotic, this effect results in beam breakup/wander in a process called scintillation. The more unstable the conditions (e.g., more negative ASTDs), the more turbulence and variability in temperature exists in individual turbulent cells. The strength of scintillation is inversely proportional to the optical wavelength (i.e., longer wavelengths are favored for EO propagation). Again, like bulk refraction, the degree of scintillation defines the relative impact of a given aerosol concentration.

Last is the issue of thermal blooming. For high intensity beams, the absorption of light by water vapor or aerosol particles is translated into heating the atmosphere. This heating, causing subsequent changes in density and refractive index, results in spatially nonuniform beam divergence. This effect in turn breaks up the beam at long range. As thermal blooming is related to absorption, it is highly dependent on beam intensity and modulation.

The relationship between aerosol particle extinction and its relative impact on specific HEL beam propagation is very complicated and is well outside this study. There is no critical value to which we can point. We are, however, concerned with simply providing reasonable aerosol scattering and absorption estimates for subsequent higher-level systems engineering studies. To this end, there are four principal aerosol species (aside from clouds) that effect near surface visibility that we need to consider: urban pollutants, biomass smoke, sea salt, and dust (technically, we should include biogenic species, but as these generally do not have a significant impact on visibility over oceans we exclude them here).

For the purpose of a HEL propagation scale analysis we will model aerosol particle properties through a bulk model surrounding particle mass concentrations, c_m. This requires four fundamental intensive parameters as a function of wavelength: 1) how much light can 1 gram of material scatter, 2) how much can it absorb, 3) in what directions is the scattered light directed, and 4) what is the effect of increased relative humidity on particle size and hence optical properties. These parameters are summarized below:

1) Description of particle extinction or scattering, such as mass extinction or scattering efficiency, α_e, α_s: Ultimately, calculations for HEL energy on target require the computation of optical depth (τ) by integrating the atmospheric extinction coefficient (b_{ext}) over the laser to target path length. As aerosol particles have a multitude of size distributions, shapes, and chemistries, there are many parameters that can be carried through to predict b_{ext}. The most convenient way to perform a first-order scale analysis is to simply study each aerosol species' mass/volume extinction or scattering efficiency (α_e and α_s, respectively). Simply put, α_e and α_s are the total light extinction or scattering cross section of 1 g of dry aerosol particles (in $m^2\ g^{-1}$). The product of α_e or α_s and the mass concentration (c_m) integrated along a path length from $x1$ to $x2$ would give the optical depth τ due to extinction or scattering of light by particles in a dry atmosphere:

$$\tau = \int_{x_1}^{x_2} \alpha_e c_m(x)\, dx.$$

Typically, α_e and α_s are measured in the visible. Extrapolations to the near IR can be made through Sun photometer measurements. Extrapolative data at longer wavelengths are rare and hence models are used to generate $\alpha_e(\lambda)$.

Frequently the wavelength dependence of extinction or scattering is reported in the literature through the Ångstrom exponent, $\alpha\lambda$, which is computed from the Ångstrom relation (Ångstrom 1929):

$$\tau = \tau_o \lambda^{-\alpha_\lambda},$$

where a is the Ångstrom exponent, λ is the wavelength (in μm), and τ_o the optical depth at $\lambda = 1$ μm. Because the wavelength dependence of extinction or scattering does not follow the above equation exactly, α can be computed for any subrange using the expression:

$$\alpha_{\lambda_1,\lambda_2} = -\frac{\ln\left(\tau_{\lambda_1}/\tau_{\lambda_2}\right)}{\ln\left(\lambda_1/\lambda_2\right)}$$

where τ_{λ_1} and τ_{λ_2} are the AOT (aerosol optical thickness) at wavelengths of λ_1 and λ_2, respectively. As particles increase in size, the value of α decreases. For example, α is ~0 for coarse mode soil and sea-salt particles and α is 1 to 3 for fine-mode anthropogenic pollutants (e.g., Tanré et al. 1988; Tomasi et al. 1983).

The Ångstrom exponent is commonly used in visible and near IR, and rarely applied directly to the infrared. However, HEL wavelengths up to ~2.2 μm can benefit from this parameterization. Analysis of longer wavelength extinction is also greatly aided by its examination because of a qualitative ability to distinguish between fine and coarse mode particles (that is, particles that have small and large effects in the IR).

2) Description of particle absorption, such as particle absorption efficiency α_a and single-scattering albedo ω_0: α_a is the total light absorption cross section of 1 g of aerosol particles. Similar to α_e and α_s, the product of α_a and c_m would give the total aerosol optical depth due to absorption in a dry atmosphere. Alternatively, instead of requiring a mass absorption efficiency, the models require the particle single scattering albedo, ω_0, defined as the ratio of particle scattering to particle extinction (the sum of scattering and absorption coefficients):

$$\omega_o \equiv \frac{\sigma_s}{\sigma_e} = \frac{\sigma_s}{\sigma_s + \sigma_a} = \frac{\alpha_s}{\alpha_s + \alpha_a}$$

3) Description of the relative direction of light scattering such as the particle phase function $P(\Theta)$. For a simple transmission calculation (say to support the computation of energy on a target) the application of the scattering phase function is not necessary. However, phase function parameterizations are required in applications where we wish to estimate atmospheric extinction from remote sensing or visibility measurements, or if one wishes to calculate atmospheric backscatter towards the HEL system itself. This work is saved for future analysis.

4) Description of the effects of increased relative humidity on particle scattering, such as the hygroscopic growth factor f(RH): A key parameter for deriving light extinction is determination of how light scattering by aerosol increases due to the geometric growth of particles at high relative humidity by to the uptake of water. The hygroscopic growth factor f(RH), often taken at RH = 80% (f(80%)), is defined as the ratio of light scattering by the aerosol at a RH of 80% to the light scattering of the dry aerosol (usually at RH< 35%), $\sigma_{s,dry}$:

$$ f(80\%) = \frac{\sigma_s (RH = 80\%)}{\sigma_{s,dry}} $$

The value of f(80%) can range from 1.1 for smoke particles to over 2 for highly soluble sulfate and sea salt (Kotchenruther and Hobbs 1998). In a generalized form, f(RH) is frequently formulated as a ratio to scattering at a relative humidity of 30% (Kasten 1969):

$$ f(RH) = \left[\frac{\left(1 - \dfrac{RH}{100}\right)}{\left(1 - \dfrac{30}{100}\right)} \right]^{-\gamma} $$

where RH is in percent and γ is an empirical fitting parameter, the value of which ranges from 0 for insoluble particles to almost 1 for highly soluble particles. The product of $f(rh)$ with α_s and c_m would give the total aerosol optical depth due to scattering in an ambient atmosphere (Note there is no hygroscopicity term for the absorption coefficient as it is fairly close to 1 for unsaturated conditions). The problem with simple parameterization such as this is that they do not take into account the hysteresis effects of hygroscopic growth. Most particles that are completely dry do not begin to grow until ~70% RH (an exception to this is acids). However, if a particle reaches ~80% RH and is then dried, it does not retrace the original curve as the water becomes relatively tightly bound. It is a rough approximation to assume that the hydrated curve is linear between 80% and 35% RH. In the marine boundary layer, it is a good assumption that the particles are well hydrated and this linear can be used.

The aerosol properties described above are less than distinctive and often co-vary. For example, increasing particle size at higher relative humidity can alter the atmospheric extinction and change the phase function and single-scattering albedo. In the following section we review these properties for urban, biomass burning, dust, and sea salt. For comparative purposes, Fig. 1 shows the wavelength dependence of extinction for these various species. Figure 1(a) gives the volume extinction efficiency as a function of wavelength, whereas Fig. 1(b) normalizes extinction at 1.06 μm.

In the following sections, we give a brief review of the properties of commonly found aerosol particles. In general, particles are divided into the fine mode (particles with diameter ~0.3 μm from combustion sources such as smoke and urban pollution) and the coarse mode (particles with diameters of about 5 to 15 μm from mechanical sources such as dust and sea salt). These discussions should be considered general enough for basic scale analysis. But, regional aerosol models are ultimately necessary and are proposed for future work.
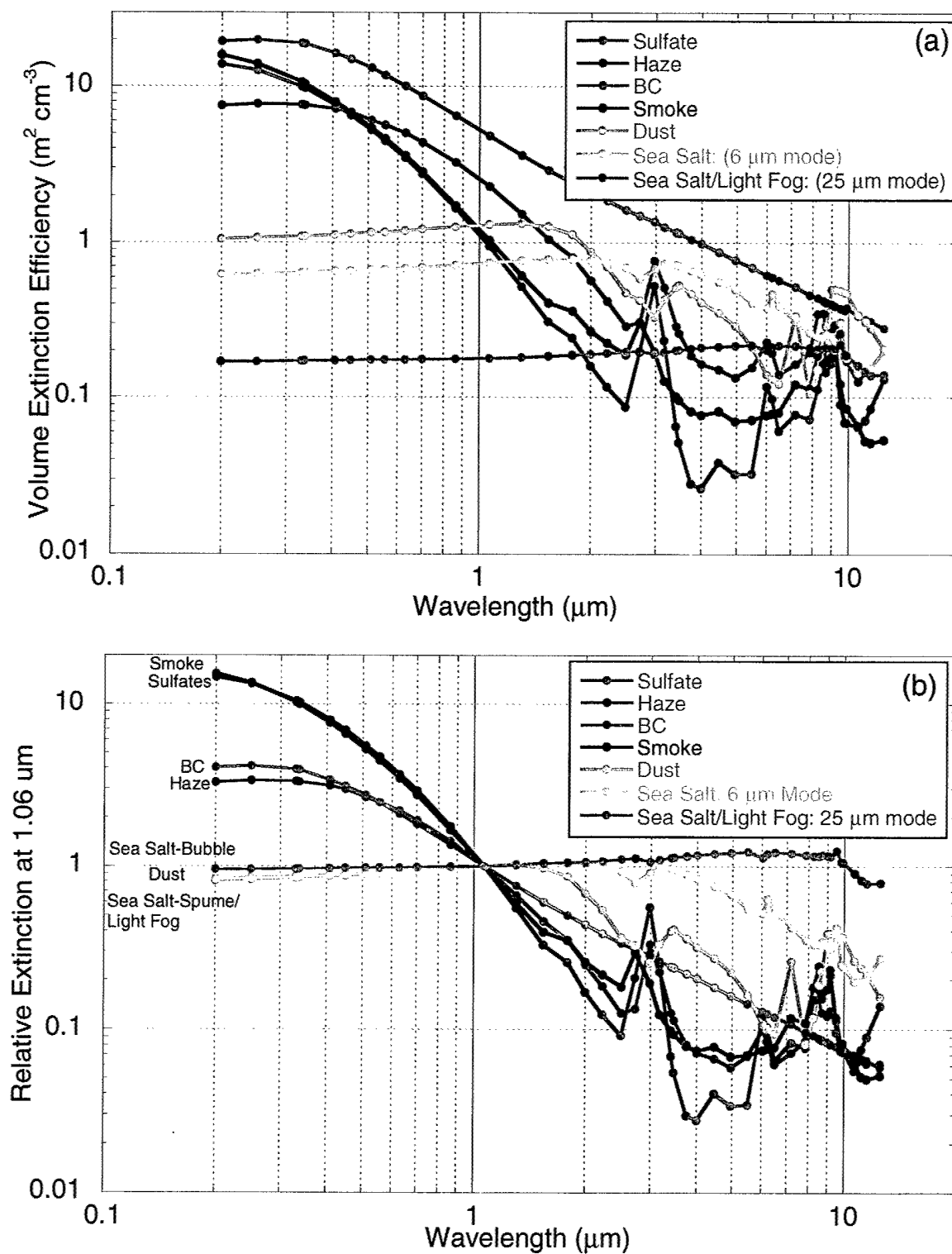
Fig. 1 — Particle wavelength-dependent scattering properties for a relative humidity of 80% (a) aerosol volume extinction efficiency and (b) relative extinction to 1.06 μm.

4.1 Sulfate and Fossil Fuel Pollutants

Urban pollution is almost ubiquitous in Earth's atmosphere, with the highest concentrations in developing economies. Historically, urban pollution studies have focused on sulfate in the form of ammonium sulfate, $(NH_4)_2SO_4$ or sulfuric acid, H_2SO_4. Since the sulfate ion itself makes up about half of the ammonium sulfate compound or can exist as the dominant pollution species sulfuric acid with tightly bound water, the term "sulfate" is often used as a surrogate for the entire aerosol species. Many global aerosol models such as NAAPS model industrial and urban emissions simply as sulfate species $(SO_4^= + n*NH_4^= + H_2O)$ or sulfate plus black carbon (e.g., soot). The difficulty in using "sulfate" as a surrogate for all anthropogenic emissions is that these species probably account for less than 1/3 of the total atmospheric load for urban pollution. In addition to sulfates, industrial pollutants include a large mix of other species, such as organic carbon, black carbon (or "soot"), and nitrates. The Intergovernmental Panel on Climate Change (IPCC 1995) estimated that globally sulfates and their associated species from SO_2 oxidation account for 45% of all urban/industrial emissions, and for ~35% of all anthropogenic emission (including biomass burning). More recent studies suggest that organic carbon concentrations may exist in much higher concentrations than expected, and hence SO_2 products may account for as little as 25% of all urban/industrial emissions. For example, Kotchenruther et al. (1999) found organic carbon often accounts for 50% of the mass of fine mode particles leaving the continental United States. Since each region of the world has its own mix of pollutants, simply allowing sulfate to be used as a proxy for all pollutants could cause very large uncertainties.

Because of air quality issues related to industrial emissions, urban pollution has received the most attention of any aerosol species. As expected, the properties of urban pollution are location specific with significant differences being found between North America, Europe and Asia. As urban pollution is for the most part from combustion sources or secondary particle production (i.e., gas to particle conversion) pollution transported out of cities is in the accumulation mode ($d_p < 1$ μm). Typically, a dry volume median diameter amounts to 0.25-0.35 μm with a geometric standard deviation of ~1.6-1.8 (e.g., Whitby 1978; IPCC 1995, 2001; Dubovik et al. 2002). As sulfate is highly hygroscopic, particles swell significantly at higher relative humidity. Using commonly accepted values of f(RH), scattering is increased on the order of factor of 1.5 to 2 for RH values above 80%, corresponding to a 50% increase in mean particle size (e.g., Tang 1996; Kotchenruther et al. 1998). When conditions are right, urban pollutants can increase in size and form thick hazes (e.g., stagnant air with high relative humidity). In such cases, core particles can grow to ambient sizes as large as 0.8 μm in diameter (Wall et al. 1988; John et al. 1990).

Light absorption by urban pollution is principally from black carbon (or "soot"). In contrast to sulfate, there is no standard definition for black carbon (BC). Novakov et al. (1982) define BC as a highly light-absorbing carbon-based material such as soot that has a graphitic like structure. Black carbon is highly absorbing compared to other aerosol species and hence is often assumed to be responsible for all short-wave radiation absorption in polluted air. Often this highly light-absorbing material is referred to as "elemental" and "graphitic" carbon, although this nomenclature is technically incorrect. There are in fact a variety of "sootlike" species that absorb light to varying degrees (Liousse et al. 1995). Like organic carbon, BC can have associated hydrogen, oxygen, and nitrogen atoms, although in much smaller percentages.

The relative amount of BC to other pollutants in the urban plume is highly variable. In western counties where clean air standards exist, controls are placed on most sources. Typically, diesel exhaust is the primary source in such regions. East Coast haze typically has a 5% black carbon content with a mid-visible dry single scattering albedo of 0.88 to 0.95 (Hegg et al. 1997; Hartley et al. 2000). However, in Asia, Eastern Europe, and most developing countries, fuel quality and efficiency are low, and few control

measures are in place. In such places BC is a much larger component of aerosol mass, and the dry single-scattering albedo is on the order of 0.8 to 0.86 (Bergin et al. 2001).

Table 1 provides a summary of relative extinction for what is typically assumed for urban pollution and haze. For comparison purposes we assume a 10 km path length along the surface for pollution and an optical depth of 1 at 1.06 µm. Also shown are conservative estimates for light absorption along the same path. Urban pollution assumes a dry particle volume median diameter (VMD) of 0.3 µm and a geometric standard deviation of 1.65. Haze conditions assume a dry particle VMD of 0.5 µm and a geometric standard deviation of 1.8. Black carbon is internally mixed and is assumed to be 8% of the dry particle volume.

Because of their relatively small size, light scattering and absorption by urban pollutants are strongly wavelength dependent. As is shown in Fig. 1, this dependence is the steepest for wavelengths around 1 µm. As particle extinction decreases with wavelength, the relative amount of absorption increases.

In reasonably polluted portions of the globe such as East Asia and the Persian Gulf, 10 km surface optical depths on the order of 1 are not uncommon (statistics given in Section 8). Under these circumstances extinction and absorption by urban pollution can easily exceed absorption by water vapor for wavelengths shorter than 2.25 µm, as shown in Table 1. During extreme haze events, relative extinction is higher and relative absorption is lower than urban pollution, due to higher quantities of non-absorbing sulfate and water.

Because of the strong wavelength dependence of scattering and absorption by urban pollution, HEL propagation is most favored at the longer wavelengths where aerosol absorption catches up with gas absorption. Table 1 lists the 10-km averaged molecular absorption coefficient assuming harsh summertime Persian Gulf conditions (this value is at the maximum of values to be found in a maritime environment). Wavelengths represent the most optimum 1 cm^{-1} band in each of the major atmospheric transmission windows as determined by MODTRAN. For a 10-km path and an aerosol optical depth of one, total extinction by particles exceeds water vapor absorption by a factor of one hundred to two out to the 2.25-µm window. This is not surprising as the majority of the potential wavelengths for HEL are picked to be in atmospheric transmission windows to begin with to reduce thermal booming.

Table 1 — Relative extinction and absorption by urban pollution. Absorption estimates are based on western countries and hence are considered conservative for most developing parts of the globe. Computation for *f*(RH) and molecular water vapor absorption assumes a harsh Persian Gulf environment of a temperature of 34 °C and a relative humidity of 80%.

Wavelength	Water Vapor (km^{-1})	Ext. Urban (km^{-1})	Abs. Urban (km^{-1})	Ext. Haze (km^{-1})	Abs. Haze (km^{-1})
0.55	--	0.40	0.024	0.24	0.008
0.67	--	0.30	0.021	0.19	0.008
1.062	0.001	0.10	0.014	0.10	0.006
1.249	0.001	0.065	0.012	0.075	0.005
1.316	0.21	0.055	0.012	0.065	0.005
1.626	0.0015	0.035	0.009	0.045	0.004
2.249	0.012	0.015	0.009	0.020	0.004
3.823	0.022	0.006	0.005	0.0095	0.005
10.449	0.74	0.006	0.006	0.0055	0.005

As thermal blooming is one of the most destructive mechanisms against HEL propagation, what may be more relevant is the comparison of aerosol particle absorption to water vapor absorption. In such a comparison, the 1.625 μm is clearly the most favored wavelength with less molecular absorption and a third of the aerosol light scattering compared to 1.06 μm. This advantage in absorption also holds for 10-km 1.06 μm optical depths of 0.5. A wavelength in the region of 2.25 μm is also a good candidate in dry atmospheres or if a very low gas absorption line can be found through HITRAN studies. The offsetting relationship between water vapor and aerosol particle absorption is a recurrent issue discussed in this report. Clearly, for an atmosphere loaded with fine mode particles, the optimum wavelength increases for lower visibility.

4.2 Smoke

Currently, biomass burning globally is at a historical high, consuming between 3,200 and 4,500 Tg of carbon annually (Crutzen and Andreae 1990) and producing a total of 104 Tg of fine particles per year (IPCC 1995) worldwide. This makes biomass burning the world's largest producer of aerosol pollutants next to sulfates (120 Tg per year) (IPCC 1995). Smoke plumes from regions of active burning reach continental scales, cover thousands to millions of square kilometers, and have been observed on every inhabited continent (Robock 1991; Westphal and Toon 1991). Aside from reducing visibility to less than 3 km for thousands of square kilometers, these smoke plumes result in noticeable decreases in surface temperatures, which might change atmospheric circulation on regional scales.

Eighty percent of the particles from biomass burning are generated in the tropics, where optical depths are frequently above one and occasionally above 3 during the burning seasons. Hence smoke particles are one of the dominant types of visibility reducing aerosol species in South America, Southern Africa, and Southeast Asia. Other notable areas impacted by burning include the Indian/Pakistani outflow into the Arabian Sea and smoke from fires on the Yucatan peninsula that is transported in the Gulf of Mexico.

Currently, the physical and optical properties of smoke particles have been measured in North America, South America, Africa and Europe. Smoke particle number and mass are overwhelmingly in the accumulation mode. Scanning and transmission electron microscopy studies have shown smoke particles to have a variety of morphologies such as chain aggregates, solid irregulars and more liquid/spherical shapes (For example, see Cachier et al. 1991, Woods et al. 1991, Gaudichet et al. 1995, Martins et al. 1996, and Reid and Hobbs 1998). As black carbon chain aggregates produced in the flame zone can serve as condensation nuclei for low vapor pressure organics that survive oxidation, it is not uncommon for micrographs to show particles as semispherical semiliquid droplets with solid complex cores. There is a trend towards more complicated shapes for vigorously flaming combustion (Martins et al. 1996). For typical grass, cerrado, and forest fires, the solid cores account for one-third to two thirds of the total particle diameter (Reid and Hobbs 1998). In extreme oxidation environments with high combustion efficiencies, uncoated chain aggregates are emitted (e.g., Cachier et al. 1991, Woods et al. 1991). Despite the ability to behave as effective cloud condensation nuclei, smoke particles have also been shown to have relatively small hygroscopic growth at high relative humidity. For example, Kotchenruther and Hobbs (1998) found that light scattering increased by a factor of 1.15 to 1.3 between dry and 80% relative humidity conditions. For a volume median diameter of ~0.3 μm, this would correspond to ~12% increase in size. For very well-aged smoke, the hygroscopic growth factor can be as high as 1.6.

Most reports on freshly emitted smoke particle give similar results, with aerosol count median diameters (CMDs) in the 0.1-0.2 μm range, centered at ~0.13 μm (see Reid and Hobbs (1998) for an overview). Volume median diameters (VMDs) are also consistent with typical values in the 0.25 to 0.3 μm range (but with some reported values as high as 0.5 μm). Geometric standard deviations for both the number and volume distributions are on the order of 1.5 to 1.9, with a reasonable mean value of ~1.7. Smoke particles grow rapidly in the atmosphere through coagulation and condensation of long chain

hydrocarbons. Secondary gas-to-particle conversion also takes place. The consequence of these processes is that smoke particle grow in size, thus increasing their light scattering and light-scattering efficiency. Aged smoke particles have a VMD on the order of 0.3 to 0.35 mm, with large haze particles occasionally being found with VMDs on the order of 0.5 μm. Particle hygroscopicity can also increase, with $f(80)$ values being reported as high as 1.5.

Relative light extinction and absorption estimates from biomass burning particles are presented in Table 4.2. Like urban pollution and haze, smoke particles are small in size and hence have strong wavelength dependence in the very near IR portion of the spectrum. Absorption is more pronounced in smoke, however, due to increased black carbon content, the focusing effects related to particle morphology, and lower hygroscopicity. The single-scattering albedo for smoke is also highly variable and is strongly dependent on the biomass fuel and burning conditions. Table 2 gives two values of smoke absorption for temperate and tropical burning.

Wavelength optimization for HEL propagation in smoke follows along similar lines as urban pollution. By moving to longer wavelengths, the scattering by these particles is greatly diminished. The higher absorption by smoke particles makes longer wavelengths more attractive. The flattening of the absorption spectrum at longer wavelengths makes 1.625 μm a clearly superior choice. Like urban pollution, selecting a wavelength in the 2.25-μm band will depend on the tolerance for absorption and thermal blooming.

Lastly, under the category of biomass burning, oil fires should also be mentioned. Burning wells significantly degraded visibility in the Persian Gulf in the months following the Gulf War, and to a lesser extent during Operation Iraqi Freedom. Oil smoke particles have little resemblance to those from burning biomass. In the hot flame zone, large chain aggregates are formed up to 10 or 20 mm in diameters. As aggregates of carbon, these particles are highly absorbing and can have large optical cross sections across wavelengths (Weiss and Hobbs 1992; Reid et al. 1994). Consequently, there are no optimum wavelengths for propagation in plumes such as this.

Table 2 - Relative extinction and absorption by biomass burning smoke assuming a 1.06 μm optical depth of 1 at 10 km. Absorption estimates are for well-aged smoke from temperate and tropical fires. Computation for $f(RH)$ and water vapor absorption assumed a temperature of 34 °C and a relative humidity of 80%.

Wavelength	Water Vapor (km^{-1})	Ext. Smoke (km^{-1})	Abs. Smoke Temperate (km^{-1})	Abs. Smoke Tropical (km^{-1})
0.55	--	0.38	0.016	0.033
0.67	--	0.27	0.016	0.028
1.062	0.001	0.10	0.014	0.018
1.249	0.001	0.061	0.013	0.015
1.316	0.21	0.052	0.012	0.014
1.626	0.0015	0.027	0.010	0.011
2.249	0.012	0.011	0.008	0.008
3.823	0.022	0.007	0.007	0.007
10.449	0.74	0.008	0.008	0.009

4.3 Airborne Dust

Airborne dust significantly impairs visibility in North Africa, Mediterranean, Southwest Asia, and East Asia on a regular basis. In many sensitive regions, such as the Persian Gulf and Yellow Sea, desert dust, in particular, significantly impairs visibility on a regular basis. Post-analysis of Desert Storm actions showed that a significant number of targets were not observable to strike aircraft due to poor visibility conditions caused by water clouds, dust, and smoke. This resulted in wasted flight time and ordnance, difficulty verifying targets, and an unnecessary risk to pilots flying in hostile territory. Additionally, dust aerosols can be present in sufficient amounts to hamper Navy surface operations. Because of their large sizes, dust particles scatter far more light in the IR portion of the spectrum than does urban pollution or smoke. Consequently, dust properties and meteorology have been of interest to Navy scientists.

The study of mineral aerosols poses four special problems for radiative transfer modeling. First, dust particle nonsphericity prevents the use of standard Mie codes to compute dust particle extinction efficiencies and phase functions. Second, dust aerosols vary in composition and size from one region to the next. Compositional variability in turn induces large perturbations in the dust's refractive index as a function of wavelength. Particle chemistries vary from region to region and, consequently, Asian dusts are quite dissimilar from those from those of the Sahara region (Ganor et al. 1991; Sokolik and Toon 1999; Gao and Anderson 2001). The study of IR properties of dust has only recently become of interest to the scientific community at large and hence the study of the impact of dust aerosols on the radiative properties of the Earth's IR window regions is a relatively young field. While there have been many studies on the composition of desert dusts, and several studies on the IR properties of key minerals, there have been relatively few studies of simultaneous measurement of ambient dust composition and IR extinction. Finally, first-order parameterizations for the identification of aerosol type (sulfate, biomass burning, dust, etc.) from satellites have difficulty in differentiating between various fine-mode aerosols and dust due to its more complicated phase function.

While extremely complicated to model and monitor with precision, the fundamental properties of dust particles are known to a degree such that a HEL scale analysis can be performed. Patterson and Gillette (1977), D'Almeida et al. (1991), and Gomes and Gillette (1993) noted similarities in dust particle size distributions measured over differing arid portions of the globe. Utilizing data from cascade impactors, these investigators found that airborne dust typically has two mass modes: a prominent giant mode with a mass median diameter (MMD) > 40 μm, and a saltation mode with a MMD between 3 and 6 μm. It has also been suggested that sometimes a third submicron mode can also be present (Gomes et al. 1990; Reid et al. 1994a). There are significant biases in particle size measurements based on different methods (see Reid et al. 2003). However, for the purposes of this scale analysis, these issues are not significant. Because particles in the giant mode fall out relatively quickly, most attention has been paid to the more transportable saltation mode in the 3 to 6 μm range. In the context of HEL propagation in marine environments, this typically is the mode that is present (with the exception of the extreme northern Persian Gulf).

With a volume median diameter on the order of 4 to 5 μm, dust is optically active throughout the spectrum and is more or less spectrally flat out to ~ 2 μm, where it begins to drop off rapidly (see Fig. 1 and Table 3). Noteworthy features include spectral absorption bands around 2.8 μm and 8 to 10 μm due to the absorption spectra of SiO_2 and other minerals. Because of the low Ångstrom exponent in the 1 to 2.2 μm range, there is no optimum wavelength for reduction of scattering in HEL beams. Furthermore, dust has no hygroscopicity to speak of and hence f(RH) can for the most part be treated as 1 (Li et al. 1998).

There are, however, some significant issues relating to absorption by dust. Up to a wavelength of ~2 μm, the principal absorbers are iron oxides and hence the iron content of dust is a good surrogate for relative absorption. The properties of hematite (FeO_2) have been studied for some time and it is well established that it is a strong absorber in the blue. Absorption diminishes rapidly at longer wavelengths. Many studies have applied the index of refraction model used in Shettle and Fenn (1979). Estimated

Table 3 — Relative extinction and absorption by airborne dust assuming a 1.06 μm optical depth of 1 at 10 km. Computation for water vapor absorption assumed a temperature of 25 °C and a relative humidity of 80%. Relative absorption values are given using the indicies of refraction from Shettle and Fenn (1979) and more updated values based on the findings of Kaufman et al. (2000).

Wavelength	Water Vapor (km^{-1})	Ext. dust (km^{-1})	Abs. Dust S&F (km^{-1})	Abs. Dust Current (km^{-1})
0.55	--	0.09	0.016	0.012
0.67	--	0.09	0.015	0.006
1.062	0.001	0.10	0.011	0.001
1.249	0.001	0.10	0.010	<0.001
1.316	0.21	0.10	0.009	<0.001
1.626	0.0015	0.09	0.007	<0.001
2.249	0.012	0.05	0.005	
3.823	0.022	0.04	0.004	
10.449	0.74	0.03	0.011	

absorption values based on this model are included in Table 3. More recent studies have shown that these indicies of refraction, as well as the commonly used values from Patterson et al. (1981), overestimate absorption by well over an order of magnitude in the near IR (e.g., see Kaufman et al. 2001). Table 3 also presents some revised (and considerably lower) values. These updated values imply that light absorption by dust can more or less be neglected and that there is no favored wavelength for HEL propagation in dusty environments.

4.4 Salt and Sea Haze

The study of the electro-optical effects of sea salt and marine aerosols has understandably received the most attention of all aerosol species by Navy research. Both fine (< 2.5 μm) and coarse mode (> 2.5 μm) sea salt is produced by the white capping of the ocean surface. As with dust, there is a great deal of variability in the reported size distribution of salt particles. Some of the variability in salt-particle fluxes and size distributions is due to variations in wind speed and wave height (Blanchard et al. 1984; Hoppel et al. 1989; Fitzgerald 1991; Porter and Clarke 1997). The vertical distribution of large sea-salt particles depends on stability and convection related to air/sea temperature differences (Fairall et al. 1983; Blanchard et al. 1984; Exton et al. 1986). For similar meteorological conditions, however, measured salt particle size distributions vary considerably in the literature (see Fitzgerald 1991 and Porter and Clarke 1997 for comparisons).

On average, there are two sea salt modes that influence propagation in the IR. The first is a 6-μm volume median diameter mode (80% RH) generated by the bursting of bubbles on white caps. This mode is highly transportable and can influence IR propagation for thousands of miles after generation. Interestingly, it is not during the high wind conditions that produce these particles that they impact EO propagation the most. High wind conditions tend to bring with it more neutral stability near the surface and relative humidity < ~85%. But, because of their intermediate size and highly hygroscopic nature (*f(RH)*>>2 for 80% RH), particles can be transported to regions of calmer winds and high RH (say under stratus decks). Under such circumstances, hazes form with considerably lower visibility.

White capping waves also produce giant sea salt particles through spume production; that is, tearing of water off the crests of waves. These particles can be over 100 μm in diameter. On average, however, their volume median diameter at 80% RH is ~25 to 35 μm. Because of the large size of spume droplets, they are not very efficiently dispersed through the atmosphere. Their relative short residence time does not

allow for significant exchange of moisture, which would reduce their size and facilitate their transport. Consequently, they are present only during high wind speed events.

In the marine environment sea salt/sea spray also differentiates itself from other aerosol species in that the ocean surface is not only a sink but also a source. Hence, the vertical distribution of sea salt near the ocean surface is more complicated than other aerosol species. Strong gradients are often present. Issues relating to this aspect are highlighted in Section 7, but the spectral properties are worth discussing here. Table 4 presents light extinction and absorption relationships for the two sea salt modes (6 μm bubble and 25 μm spume). As can be seen in Figure 4.1, the large size of sea salt makes light scattering as a function of wavelength relatively flat, with an Ångstrom exponent on the order of 0.3. Light absorption is also extremely weak for all but the largest drops and longest wavelengths and can be neglected relative to water vapor. Hence, as with dust there is not a single optimum wavelength for propagation for wavelengths less than 2.25 μm.

It is noteworthy that the wavelength dependence presented in Table 4 is less than what would be produced by the Navy Aerosol Model or even the Advanced Navy Aerosol Model (ANAM). There are two reasons for this. First, NAM and ANAM place the bubble mode a factor of 4 too small at 1.5 μm. This smaller volume median diameter causes a drop-off in extinction for wavelengths greater than ~3 μm. Secondly, the models include an Air Mass Parameter (AMP) to account for the presence of urban pollution that is advected into the marine environment. The use of an AMP modulates the finer mode pollution term, which, as discussed earlier, has strong wavelength dependence around 1 μm. As we deal with the pollution term separately, it is excluded in this analysis.

5. COMPILATION OF VISIBILITY OBSERVATIONS (PAULUS, REID, MOISION)

On typically a 6-hour basis, airports and civilian and navy ships report weather conditions including surface visibility. For this study we intend to use these data sets and derive local climatologies of visibility. The purpose of this study is to examine visibility ranges, obstructions, and spatial and temporal trends to get a qualitative assessment of the periods when EO propagation is generally fair or poor. Work focused on specific regions of interest: the Persian Gulf and northern Arabian Sea, the Red Sea, the Mediterranean and Black Seas, the eastern coast of Asia, and the South China Sea.

Table 4 — Relative extinction and absorption by sea salt for both the 6-μm bubble and 25-μm spume volume modes. Computation for f(RH) and water vapor absorption assumed a temperature of 25 °C and a relative humidity of 80%.

Wavelength	Water Vapor (km^{-1})	Ext. Bubble (km^{-1})	Abs. Bubble (km^{-1})	Ext. Spume (km^{-1})	Abs. Spume (km^{-1})
0.55	--	0.09	<0.001	0. 10	<0.001
0.67	--	0.09	<0.001	0. 10	<0.001
1.062	0.001	0.10	<0.001	0.10	<0.001
1.249	0.001	0.10	<0.001	0.10	<0.001
1.316	0.21	0.10	<0.001	0.10	0.001
1.626	0.0015	0.10	<0.001	0.10	0.002
2.249	0.012	0.01	<0.001	0.11	0.004
3.823	0.022	0.09	0.002	0.11	0.01
10.449	0.74	0.02	0.009	0.10 .	0.03

The use of visibility to derive an exact aerosol light extinction number is problematic. First, despite WMO, NOAA, and Navy protocols, visibility is reported differently by many locations. By its nature, visibility is a qualitative judgment by the observer. Reporting bins are coarse, and visibility becomes more difficult to judge in the critical 10 to 20 km range. Even within the protocols, significant differences exist between the U.S. Navy and NOAA reporting requirements. As visibility is defined as a minimum detectable contrast by a detector (assumed to be the human eye), by definition it is dependent on the observer. Path radiance (i.e., solar zenith angle) effects can also be significant.

Biases have been noticed between automated and human data sets and differences exist between coastal shore-based climatologies and shipboard observations in the immediate area. There are many reasons for this. First, strong spatial gradients in aerosol particle concentration often exist in coastal regions. Further, shore-based observers are better trained than their shipboard counterparts or more objective (shipboard observations are typically made by the quartermaster). More objective automated visibility instruments are also used at shore facilities. These instruments estimate visibility by the detection of scattered light at some forward-scattering angle and, hence, are easier to relate to atmospheric extinction (however, as these systems are calibrated for fog, biases develop during severe visibility degradation due to such species as urban pollution or dust). Human observers have even more difficulty since visibility is more or less subjective. This can become serious at nighttime or over the ocean when there are no observable targets. Human observers also perform a "spatial" average at observing times while automated systems give a temporal average at some point in space. In all cases, unless the aerosol species is known, it is difficult to apply observations to the IR.

Despite these shortcomings, visibility reports are one of the few quantities related to aerosol extinction available for a near-surface extinction analysis over most of the world (e.g., Husar et al. 2000). For the first year of this project, the visibility data were only to be compiled; analysis and integration with other products were to occur at later stages. However, in this report we give an overview of some basic findings and emphasize the fraction of time visibility is less than 10 km (i.e., the horizon is obscured). Data should be considered qualitative, but representative of the probability of severe visibility-reducing events that would significantly hamper HEL propagation. Refining these analyses and relating findings to the meteorology of the region is a goal of future study. Some regions, such as the Mediterranean and East Asia, clearly need further research with the addition of remote sensing and lidar data available to the scientific community.

5.1 Visibility Data

This analysis concentrated on ship observations. Data for the period of 1960 to 1997 were provided by the Fleet Numerical Meteorology and Oceanography Detachment Asheville colocated with the National Climatic Data Center, Asheville, North Carolina. Visibility data were organized by area and season. Climatological seasons were defined as spring (March, April, May), summer (June, July, August), autumn (September, October, November), and winter (December, January, February). All data entries with valid visibility data were retained and the code value for visibility in the data set was converted to meters according to Table 5. In compiling statistics, all visibilities of 1 km or less were binned together. Observations were relatively evenly distributed over the four synoptic observations times of 00Z, 06Z, 12Z, and 18Z, although there tended to be more daytime observations than nighttime. Histograms of visibility by synoptic hour did not show any day-night bias in the data.

Table 5 — Conversion of Coded Visibility Range and Type

Data Set Visibility Code	Description	Description (distance in nmi)
Range		
1	< 50 m	< 0.027
2	50-200 m	0.027-0.11
3	200-500 m	0.11-0.27
4	500-1000 m	0.27-0.53
5	1-2 km	0.53-1.08
6	2- 4 km	1.08-2.16
7	4-10 km	2.16-5.4
8	10-20 km	5.4-10.8
9	20-50 km	10.8-27
10	50+ km	27+
Code		
00 to 03 and 13 to19	No Precipitation	
4	Smoke	
5	Haze	
06 to 09 and 30 to 39	Dust/Sand	
-0	Mist	
11 to 12 and 40 to 49	Fog	
20 to 29	Recent Precipitation	
50 to 59	Drizzle	

Visibility is difficult to measure at sea because of the lack of distance reference points. NAVMETOCCOMINST 3144.1 (series) and National Weather Service Observer's Handbook #1 provide guidance on estimating visibility at sea. The coarseness of the visibility code intervals tends to be consistent with the ability to estimate visibility without the benefit of reference targets as are present on land (Table 5). In the absence of any other references, the observer will estimate visibility based upon the sharpness and clarity of the horizon. However, in coastal environments there are often other reference points such as other ships, landmasses, and lights. The distance to the horizon for typical commercial and military shipboard observer heights is ~10 km or more. Because of the strong gradients in particle concentration over the ocean surface, viewing geometry must be considered. Refraction effects result from vertical gradients in temperature and humidity, which in turn are affected by the waves and, at higher wind speeds, evaporating aerosols. Refraction effects include image distortion, the occurrence of mirages (false alarms), dark zones (reduced range) and/or an increased detection range. While refraction is not part of this study, for the purposes of HEL propagation assessment a quick calculation and scale analysis for the distance to the optical horizon is required. The maximum detectable range for a target (at a specific height as seen by a camera at a specific height) as a function of air sea temperature difference is given in Table 6.

For standard shipboard level (say, 10 m), the geometric horizon is ~11 km. In the NOAA observing manuals, tables of geometric horizon are given to aid mariners. However, Table 6 clearly shows that refraction can lengthen or shorten this distance to the horizon dramatically. Hence, there is inherent uncertainty in using the "see the horizon" test that is commonly used by mariners. Shore-based observation have no such issue as visibility is either determined with an automated system or by use of landmarks of known distance.

Table 6 — Changes in optical horizon and maximum detectable target distance as a function of camera (H in meters) and air sea temperature difference (ASTD in Celsius). Given are the geometric horizon (in kilometers), and the maximum distance to target for a height of 0, 5, and 30 m above the water (e.g., 0 /5/30). For positive ASTDs, super-refraction occurs and maximum target distance is unlimited.

H (m)	GeoH (km)	-5	-2	ASTD 0	2	5
5	8.1	2/9/21	3/11/23	4/13/26	14//	28//
10	11.4	4/13/26	5/14/27	7/16/29	19//	39//
15	13.9	6/16/29	7/17/30	9/18/32	23//	45//
30	19.7	10/21/35	12/23/36	16/25/38	29//	45//

In the visibility data archive, data are recorded as one of the codes in Table 5. The U.S. Navy and NOAA have different protocols for "unrestricted" visibility. The maximum visibility reported by commercial vessels is typically greater than 11 nmi or 20 km (code 9). However, US Naval vessels report no greater than 10 nmi, or ~18.5 km and any visibility greater or equal to 9 nmi is reported as code 8. Hence, if all data in the climatological database are taken on an equal footing, data in code 8 is biased high relative to code 9 (e.g., biased towards worse climatology) due to the presence of U.S. Navy data. After discussions with personnel at Fleet Numerical Meteorology and Oceanography Detachment Asheville, it is our opinion that this is likely only a small bias and is taken into account in our analysis.

The 10-km range (visibility code 8) is approximately the upper limit of when obstructions to visibility must be reported (an obstruction to visibility must be reported if visibility is less than 6 nmi). However, weather phenomena that may cause obstructions to visibility may be reported even if visibility is greater than 6 nmi. Statistics were also determined by cause of obstruction. Data for this analysis was a subset of the full visibility data set, as observations that did not have temperature, pressure, relative humidity, or weather code were removed. Then the 100 currently used weather codes were categorized as listed in Table 5. Statistics for the percent occurrence of the weather categories were compiled and analyzed for each research area for each season.

Commonly, visibility and atmospheric extinction are related through the Koschmieder equation, which defines visibility as the point where the human eye can detect a 2% contrast:

$$b_{scat} = \frac{-\ln(0.02)}{Visibility} = \frac{3.9}{Visibility}.$$

So, for example, a visibility of 10 km implies a mean extinction coefficient of 0.39 km^{-1} and an optical depth of 3.9 along a 10-km path averaged over visible wavelengths. Also, because of reporting practices, a reported 10-km visibility (code 8) can really be anything between 10 and 20 km. Spatial inhomogeneity and path radiance (i.e., Sun angle) also cause a deviance from the standard Koschmieder equation. To account for all of these issues, a ratio of 1.9 instead of 3.9 is sometimes used for land-based sites (e.g., Griffing 1980). In this circumstance, a visibility report of 10 km implies the visibility is between 10 and 20 km at the observing location, a mean visible extinction coefficient of 0.19 km^{-1}, and an optical depth of 1.9 along that 10 km path. Application of this value is probably conservative over ocean where the air-sea temperature difference is typically negative (unstable conditions) and hence the true optical horizon is closer than what is listed in the NOAA and Navy manuals. The exception is very near the coast of deserts during summer where the air-sea temperature difference is positive.

Because the relationship between visible and IR extinction varies with aerosol species, there is no easy way to infer IR extinction. In the following analysis, we concentrate on two visibility categories. First, visibility category 8 (visibility between 10 and 20 km) is listed and interpreted as the fraction of time in which aerosol particles will influence HEL propagation. As discussed in the previous section, dust, sea salt, and precipitation have spectrally flat extinction. Hence, visibility category 8 also implies the fraction of time when aerosol extinction at 1.06 μm is greater than 0.19 km^{-1}, or roughly a 10-km optical depth of 2. For cases of fine mode pollution such as smoke or sulfate with a spectrally changing extinction, these numbers should be reduced by roughly a factor of 4. This translates to a 1.06-μm extinction of 0.05 km^{-1} or a 10-km optical depth of 0.5.

We also list the fraction of time in which visibility is less than 10 km and interpret this as the fraction of time aerosol particles are likely to impair laser propagation. In this case, we will err on the side of conservatism and assume 1.06-μm extinction of 0.4 and 0.1 km^{-1} for coarse and fine mode particles, respectively.

For comparison, we also list visibility estimates of coastal surface stations where visibility is less than 10 km (<5 nmi). In some cases, we have had to rely on the "flying weather" statistic (<5 mi and/or cloud deck less than 5000 ft). These cases are noted.

5.2 Persian Gulf and Northern Arabian Sea

Because of its relevance to the DoD community, the Persian Gulf region received the most attention in this study. A description of the sea/ocean sub-areas used in this analysis of data for the Persian Gulf/Arabian Sea is shown in Table 7 and in Fig. 2. Table 7 shows the percentage of time that visibility is between 10 and 20 km and <10 km by season and geographic area. Of all of the regions in which the U.S. Navy will likely use a HEL-type system, the Persian Gulf is clearly one of the most inhospitable. The hot dry air masses from the deserts quickly increase in specific humidity due to the enormous latent heat fluxes from the +25 °C ocean surface. Turbulence and refractive effects are also likely to be episodically severe along the coast. Summertime visibility in the region is among the worst in the world.

The Persian Gulf suffers from poor visibility throughout the year, particularly in the northern regions. The most notable seasonal trend is the degradation of visibility during the summer season when visibility in all regions is less than 20 km, 50% or more of the time. Hence, on average in the summer months, observers have difficulty viewing the horizon. Conversely, the best propagation conditions are clearly in winter. This annual cycle is consistent with near by shore-based observations. For example, Bahrain Airport, Kuwait airport, and Bander Abas (Iran) report visibility less than 5 nmi (<10 km) at roughly 50% and 25% of the time for July and January, respectively.

Considering that the Persian Gulf is essentially an enclosed sea it is understandable that it suffers from poorer visibility, and is climatologically distinct from the Arabian Sea. Poor visibility in the gulf is not typically from "weather" phenomenon as much as from haze and dust. This is due to the high degree of industrial pollution related to the oil industry, and the frequent dust storms that are prevalent from late spring through early fall. As there is typically a northerly component to the wind, there is a strong north/south gradient in light extinction from pollutant dispersal and, in the case of dust, sedimentation. The properties of this urban/industrial pollution are not well characterized, but, as they are from refining, light industry, and uncontrolled auto exhaust, their absorption properties are probably higher than the values given earlier in this report.

In the summertime, 75% and 15% of the cases of reported visibility obstruction were from haze and dust, respectively. The determination of "haze" or "dust" is not distinct. Hazes can be a result of dust production hundreds or even thousands of kilometers away. This can be observed in Fig. 2 where the frequency of haze is plotted against dew point depression for the Persian Gulf and the Arabian Sea.
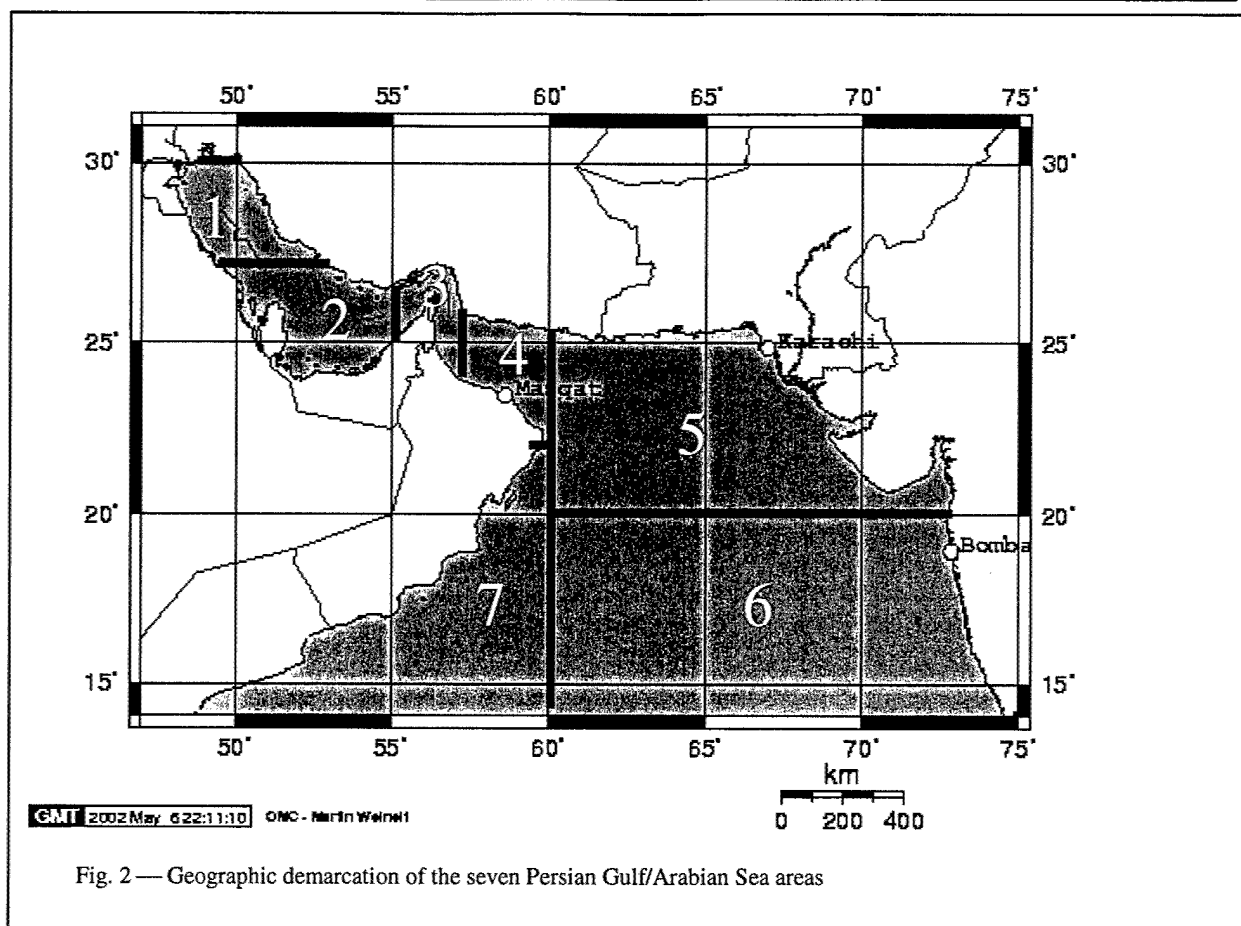
Fig. 2 — Geographic demarcation of the seven Persian Gulf/Arabian Sea areas

Clearly, haze is often found in relatively dry air masses in the Persian Gulf, suggesting dust as a significant constituent. Local observations of optical depth from Sun photometers supports this view, with 80% of the column burden particle extinction in the mid-visible being from coarse mode dust particles. It is well known that the bulk of the aerosol particles during the summer time are from dust, and daytime-northwesterly Shamal dust storms out of Iraq are not uncommon. As dust is spectrally flat between visible and near-IR wavelengths, these poor visibilities during the summer clearly extend to near-IR wavelengths in the Persian Gulf. As dust storms originate in the northern Persian Gulf more often, there is a north-south gradient in dust concentrations at the surface.

In the winter and early spring, most aerosol impacts are typically from fine particles. In such cases, the extinction coefficient is three times lower in likely HEL wavelengths. Even so, because of the absorption properties of these particles, aerosol absorption may be greater than water vapor absorption.

The cleanest region in the area is the western Arabian Sea, which only experiences visibility degradation in summer. This correlates to the increase in occurrence of mist and haze as a result of the onset of the southwest monsoon over the Arabian Sea. Stratus decks are common on the coast of Oman and Yemen in the summer months. This is supported by an analysis of dew point depression for the northern Persian Gulf and the western Arabian Sea in Fig. 3, where the dew point depression histogram for the western Arabian Sea has a median less than 5 C, and high kurtosis indicating moist conditions. Hence this region is significantly impacted due to sea haze/stratus clouds associated with the southwest monsoon. As with dust, the scattering of sea salt/haze and light fog/mist is spectrally flat, and we predict severe HEL impacts due to light scattering.

The Northern Arabian Sea along the Indian subcontinent and Strait of Hormuz also tends to have better visibility than the more restricted Persian Gulf. However, the propagation environment is considerably more complicated. Like the western Arabian Sea, stratus decks can be found, however, aerosol particles are transported in from many directions. The region is subject to upper level transport of smoke and industrial pollution from India and Pakistan. The northern coastal waters of the Arabian Sea through the Strait of Hormuz are impacted by dust from Afghanistan as well as from the Persian Gulf region.

The Persian Gulf region also has the strongest shore/sea reported visibility differences of the regions we studied. For example, while the summer time probability of visibility <10 km is only ~9% for sea based measurements, the Bahrain and Bander Abas shore stations give values on the order of 60% or a factor of 8 difference. Other shore stations are also higher by a factor of 3-5. This trend remains even when ocean data around the station are grouped for only cases within 1 degree of latitude and longitude. This should not be interpreted as a difference in a factor of 3-8 in extinction, however. Likely, the bias is small, but it does demonstrate the high probability of visibility right around the 10 km cutoff point.

There are both physical and artifact reasons which may explain this difference. Clearly, the lack of any environmental controls on combustion makes cities in the region highly polluted. This pollution can disperse fairly quickly as an air mass is advected out to sea. Hence, by this hypothesis, there should be a very strong shift in visibility very near the coastline (on the order of 20 km). On the other hand, this may indicate a general bias in ocean observation data due to refraction effects and or a lack of good visibility targets. Both physical and artifact processes are likely at work. Communications with FNMOD Ashville indicate their confidence is higher with shore station data. Regardless, the shore and ocean data should be regarded as the upper and lower bound of what likely exists in the region.

Table 7 — Definition of Persian Gulf study areas and percent occurrence of visibility. For oceanic regions, given in the fraction of time visibility is less than 10 km followed by percentage of time visibility is between 10 and 20 km (separated by a colon). For coastal cities data is taken from the FNMOD Asheville, NC Middle East climatology of visibility <10 km only.

| Area	Latitude Bounds	Longitude Bounds	Geographic Area	Spring	Summer	Fall	Winter
PG1	27N to 30N	47E to 53E	Northern Persian Gulf	10:34%	9:45%	4:27%	4:27%
PG2	24N to 27N	50E to 55E	Southern Persian Gulf	6:37	9:51	3:30	3:26
PG3	25N to 28N	55E to 57E	Straits of Hormuz	5:30	9:47	3:24	2:16
PG4	22N to 26N	57E to 60E	Gulf of Oman	2:23	7:50	1:18	1:11
PG5	20N to 26N	60E to 75E	Northern Arabian Sea	2:18	8:55	1:16	1:11
PG6	14N to 20N	60E to 75E	Arabian Sea	0.7:10	6:47	2:13	1:9
PG7	14N to 22N	47E to 60E	Western Arabian Sea	1:10	12:59	1.3:15	1:6
PG 1			Kuwait City Airport	30%	36%	20%	22%
PG 2			Bahrain Airport	34%	62%	30%	25%
PG 2			Doha, Qatar	10%	26%	10%	10%
PG 3			Bandar Abas, Iran	37%	60%	33%	21%
PG 3			Al Khasab, Oman	4%	8%	17%	4%
PG 7			Masira, Oman	5%	42%	5%	3%
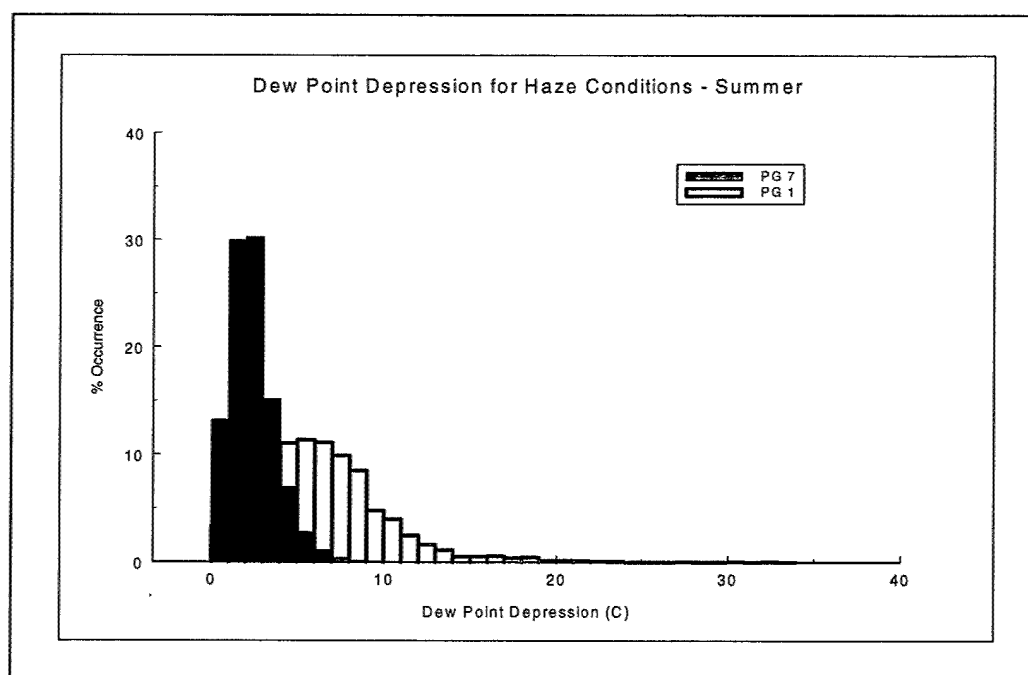
Fig. 3 — Histogram of dew point depression for northern Persian Gulf (PG1) and western Arabian Sea (PG7)

5.3 Red Sea

Regions of interest for the Red Sea are presented in Fig. 4, with summary findings presented in Table 8. The Red Sea is a common shipping lane for commercial and military traffic. Because it is isolated from industrial centers, visibility in the region is considerably better than in the Persian Gulf. The wintertime EO propagation environment is generally good with occasional occurrence of poor visibility due to haze (~13%), and occasional mist. Like the Persian Gulf, haze is not very specific and is often a product of transported dust. The Red Sea haze is persistent throughout the year, and is a maximum during the summer. Dust/sand also peaks in the summer time with visibility being below 10 km for 1/3 of the time. This is consistent with what is known of the meteorology of the region, with local dust often mixed with dust generated in the central Sahara. As reduced visibility is mostly from dust, poor visibility in the visible extends directly to the near-IR portions of the spectrum. Regardless, severe events occur only about 20 times per year. As in the Persian Gulf, there is a difference between the ocean and shore-based visibility estimates.
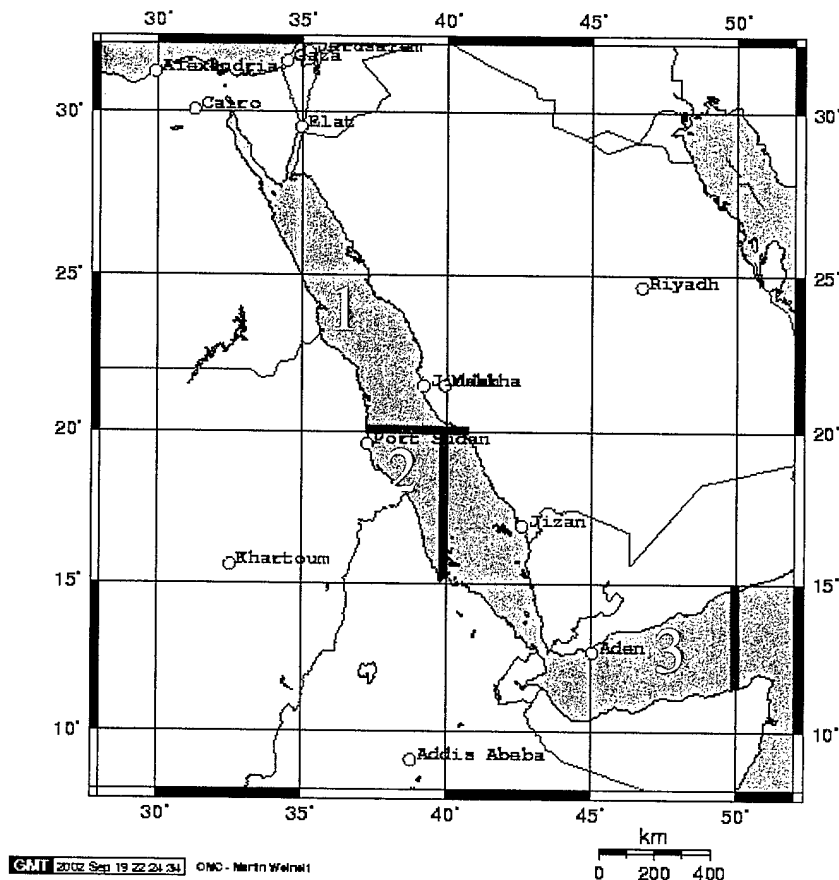

Fig. 4 — Geographic demarcation of the three Red Sea areas

Table 8 — Definition of study areas in the Red Sea and percent occurrence of visibility. For oceanic regions, given in the fraction of time visibility is less than 10 km followed by percentage of time visibility is between 10 and 20 km (separated by a colon). For coastal cities, data are taken from the FNMOD Asheville, North Carolina. Middle East climatology of visibility <10 km only.

Area	Latitude Bounds	Longitude Bounds	Geographic Area	Spring	Summer	Fall	Winter
RS1	North of 20N	Land	Northern Red Sea	3:21%	4:27%	2:19%	1:10%
RS2	15N to 20N	West of 40E	Central Red Sea	3:21	10:28	2:27	1:13
RS3	South of 15N	40E to 50E	Southern Red Sea	2:15	7:31	1:12	1:12
RS2			Port Sudan, Sudan	10%	22%	7%	7%
RS3			Aden, Yemen	4%	36%	8%	3%

5.4 Mediterranean and Black Sea

The Mediterranean and Black Sea regions are complicated and can be difficult to characterize in terms of EO propagation. The numerous seas and orographic features produce a multitude of regional subclimates. Bounded on the south by the deserts of North Africa and on the north by Western and Eastern Europe, every category of aerosol species is present somewhere in this region at almost any time of the year. Summary regions of interest and visibility degradation statistics can be found in Fig. 5 and Table 9.

Throughout the year, Mediterranean regions have degraded visibility (<10 to 20 km) at least one out of every 5 days, with seasonal maxima of at least 1 out of every 3 days. The best visibilities occur in late fall and winter when the weather is dominated by precipitation. The most notable seasonal trend is the degradation of visibility during the spring and summer seasons, when visibility in the Gibraltar, western, central, and eastern Mediterranean regions is 10 km or less more than 35% of the time.

Visibilities in the Black Sea are degraded to less than 10 km for 1 out of every 5 days in winter and spring, the result of precipitation coupled with extreme wintertime pollution in that region. Visibility tends to be best in the summer and fall, but is still degraded more than 35% of the time, due primarily to Eastern European pollution.

The complexity of the meteorology and air masses of the Mediterranean and Black Sea region makes extrapolating visibility data to HEL wavelengths a challenge and requires more study from remote sensing and modeling methods. The commonly identified "haze" categorization is clearly not specific enough. As in the Persian Gulf and Red Sea, transported dust is commonly placed in this category. There are three principal source regions that impact this area. First, dust produced in the interior of the Sahara is transported westwards over the Cape Verde Islands and Tenerife. This dust can then be transported north, be caught in the westerly winds, and advected across Gibraltar and Great Britain. Dust from Libya is directly transported over the Mediterranean between Italy and Crete. Finally, dust from Israel, Syria, and Jordan is occasionally transported westward into the Mediterranean. Significant dust storms from at least one of these mechanisms affect the Mediterranean at least every two weeks. For such dust events, extrapolation of visibility would translate directly to the near-IR.

Pollution impacts are also complicated. Controls on pollution and fossil fuel efficiency show a strong gradient as one moves eastward through Europe. Western countries' air quality regulations have reduced the amount of pollution emitted, particularly black carbon. However, Eastern Europe has only begun such control measures. After the fall of the Eastern Block in the early 1990s, many industries used poor grade

coal (essentially high grade peat) to fuel boilers. This fuel produced massive emissions of black carbon that significantly absorbed light (even in the near IR). Western investment in the region has improved the situation, but more absorbing pollution is still prevalent.

The region that most restricts EO propagation is the Adriatic. This region is commonly impacted by sea haze and pollution (particularly in the summer) with occasional injections of dust and biomass burning smoke. Stratus clouds are also common in the region and likely modulate much of the visibility degradation. Like all regions, shore-based visibility is substantially lower than estimates from ships.
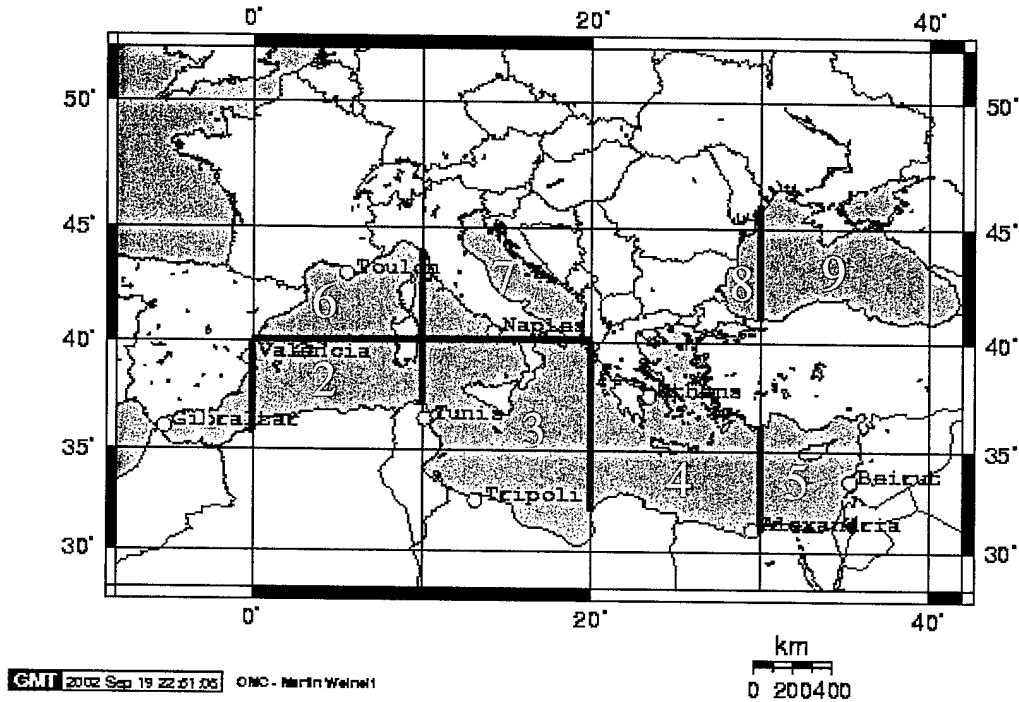

Fig. 5 — Geographic demarcation of the nine Mediterranean/Black Sea areas

Table 9 — Mediterranean visibility statistics. For oceanic regions, given in the fraction of time visibility is less than 10 km followed by percentage of time visibility is between 10 and 20 km (separated by a colon). For coastal cities, data are taken from the FNMOD Asheville, NC climatology of visibility <10 km only. * Indicates values are for visibility <10 km and/ or cloud below 5,000 ft.

Area	Latitude Bounds	Longitude Bounds	Geographic Area	Spring	Summer	Fall	Winter
MED1	land	West of 0	Gibraltar/Alboran	5:26%	11:36%	5:4%	3:17%
MED2	S. of 40N	0 to 10E	Western Mediterranean	5:28	7:32	3:20	3;19
MED3	S. of 40N	10E to 20E	Central Mediterranean	5:31	5:34	3:22	3:20
MED4	S. of 41N	20E to 30E	Central Mediterranean	3:30	4:44	2:23	3:19
MED5	land	E. of 30E	Eastern Mediterranean	3:26	4:33	2:19	3:17
MED6	N. of 40N	0 to 10E	Northwest Mediterranean	6:34	6:34	5:30	5:30
MED7	N. of 40N	10E to 20E	Adriatic/Tyrrhenian	8:44	6:45	7:40	8:39
BS8	land	W. of 30E	Western Black Sea	24:40	7:31	11:38	19:36
BS9	Land	E. of 30E	Black Sea	23:34	8:36	7:27	16:36
MED3			Tripoli, Libya	18%	12	10	12
MED4			Iraklion, Crete	2	1	1	2
MED4			Souda Bay, Crete	4	1	4	4
MED5			Beirut, Lebanon	6	3	3	5
MED7			Brindisi, Italy	30	24	29	30
MED1			Barcelona, Spain*	37	32	38	35
MED6			Nice, France*	24	18	23	24
MED6			Toulon, France*	24	17	28	29

5.5 Asia

Like the Mediterranean and Black Sea region, Asia is a very complicated region for assessing EO impacts by aerosol particles and weather. East Asia covers 70 degrees of latitude, from the near polar to the tropics. Each longitudinal band has fundamentally different meteorology and aerosol properties. Because the economies of the counties in this region are growing so rapidly, it is a region of interest by the entire climate community. Frontal systems, tropical cyclones, and other weather phenomena produce a large quantity of precipitation in the Asian coastal waters. By nature, the region is heavily polluted by fossil fuel emissions and biomass burning smoke. Dust is frequently advected out to sea from the Gobi and Taklamakan deserts.

The description of the sea/ocean subareas used in this analysis for the East and Southeast Asian coastal area is shown in Table 10 and in Fig. 6. A cursory examination of Table 10 shows why there is so much concern in the scientific community. Visibility in the mid latitudes drops below 10 km roughly 1 out of 3 to 8 days throughout the year. There are also visible seasonal trends in each region. Off all of the areas examined in this report, the East and Southeastern Asian theaters require the most study. Winter, spring, and summer stand out as having the poorest propagation conditions throughout the region. North of 30N,
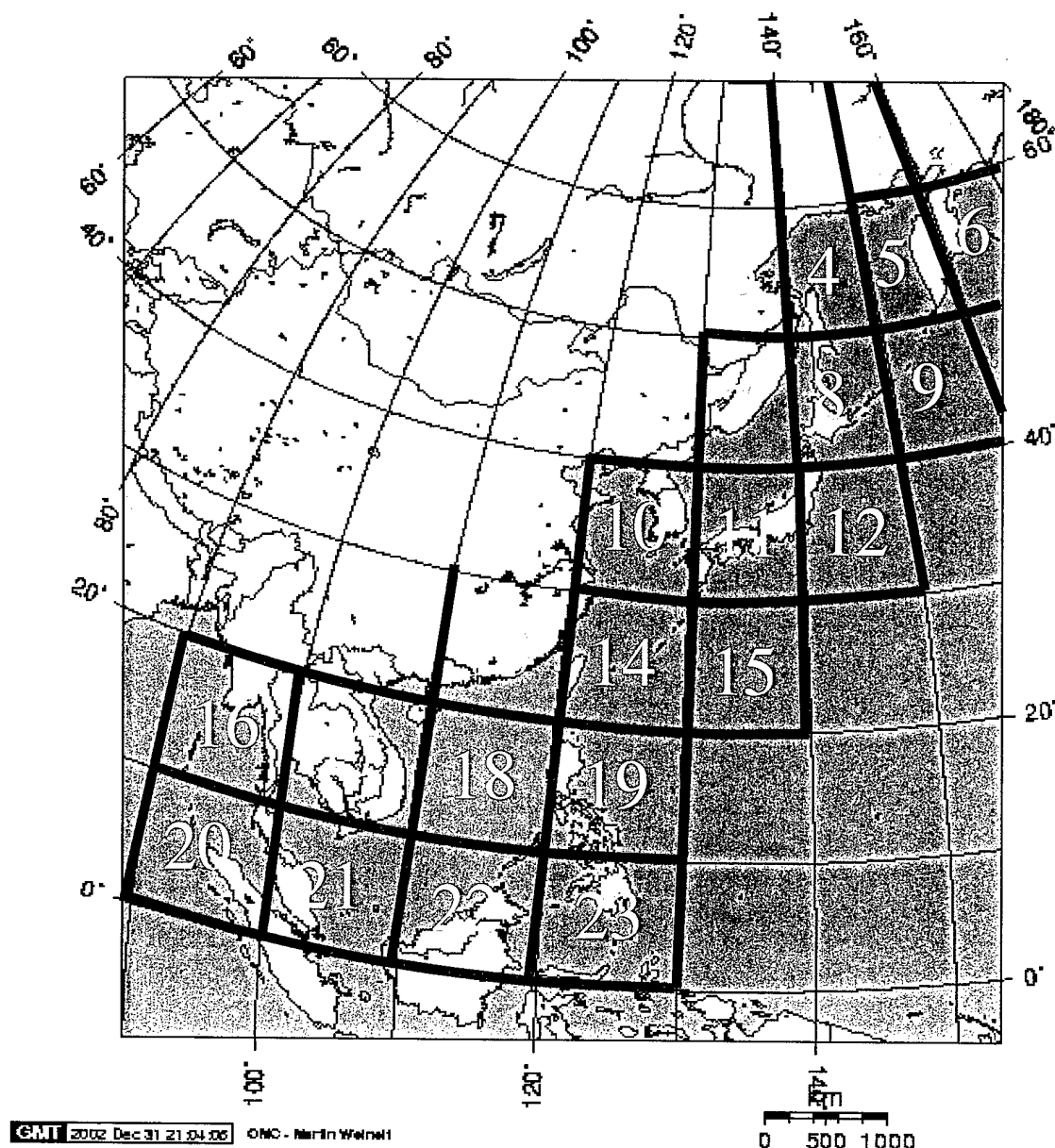
Fig. 6 — Geographic demarcation of the 23 east and Southeast Asia areas

autumn is the season that stands out has having the lowest occurrence of visibilities of less than 20 km. Even so, only the northern Sea of Japan has occurrence significantly less than 30% of the time. Summer tends to be the season with the greatest occurrence of low visibilities, but is not markedly so. In the sub-tropical latitudes of 20N to 30N (Asia 13, 14, 15), the occurrence of low visibilities is worst in spring, and best in summer. In the tropical latitudes, between the equator and 20N (Asia 16-23), spring tends to be the season of least occurrence of low visibilities, and winter the season with the greatest occurrence, though this is not consistent throughout the region. There is a strong latitudinal variation, with better visibility in the tropical latitudes.

The histograms of obstructions to visibility show precipitation to be the most common cause of obstructions to visibility over the Asian coastal regions. Fog is the dominant obstruction to visibility in the East Asia area in summer, arising mainly in the ocean areas (Asia 1-6 and 8-9) to the north of the

Kuroshio Current. In spring and fall, the most common visibility obstructions are also fog and precipitation. In the winter, fog diminishes and precipitation becomes the dominant obstruction to visibility. There is a surprising lack of dust or haze classifications for obstructed visibility in the region. It is well known, however, that dust events are a common place in the spring, and that there is a pollution maximum in summer. These events are so intense that it is not unreasonable to assume that some of the fog categorizations are actually from these other sources.

In the Southeast Asia area, haze and precipitation are the main obstructions to visibility, and show no distinct temporal trend. Haze likely takes several forms. First, as with all developing regions, Southeast Asia is fairly polluted. Biomass burning smoke from deforestation and agriculture commonly pollutes the regions around Thailand and Vietnam in the spring. Burning is also prevalent in Indonesia, Java, and Borneo. With the haze likely being in these forms, optical depths in the infrared will be reduced by a factor of three. As this is a tropical area, thunderstorms are fairly common, and carry the potential to reduce visibility to low levels in the summer. Because of the warm sea surface temperatures in the tropical regions, water vapor absorption is relatively high.

Shore-based visibility is also a factor of two to three lower than ship observations. Because of the extreme amount of pollution generated in Asia, a large fraction of this difference is probably real.

Table 10 — East Asia visibility statistics. For oceanic regions, given is the fraction of time visibility is less than 10 km followed by percentage of time visibility is between 10 and 20 km (separated by a colon). For coastal cities, data are taken from the FNMOD Asheville NC climatology of visibility <10 km and/ or clouds below 5,000 ft.

Area	Latitude Bounds	Longitude Bounds	Geographic Area	Spring	Summer	Fall	Winter
Asia1	N. of 60N	W. of 160E	Sea of Okhotsk*	20:18%	19:21%	14:17%	24:18%
Asia2	N. of 60N	E. of 160E	Sea of Okhotsk*	20:18	19:21	14:17	24:18
Asia3	50N to 60N	W. of 140E	Sea of Okhotsk*	21:21	19:23	16:20	28:20
Asia4	50N to 60N	140E to 150E	Sea of Okhotsk*	21:21	19:23	16:20	28:20
Asia5	50N to 60N	150E to 160E	Sea of Okhotsk*	20:18	19:21	14:17	24:18
Asia6	50N to 60N	160E to 170E	Eastern Kamchatka Peninsula	21:20	20:22	14:21	26:23
Asia7	40N to 50N	130E to 140E	Northern Sea of Japan	13:20	18:24	7:15	12:17
Asia8	40N to 50N	140E to 150E	Sakhalin/Hokkaido	18:22	21:24	12:20	20:21
Asia9	40N to 50N	150E to 160E	Kuril Islands	26:28	29:29	18:25	27:29
Asia10	30N to 40N	120E to 130E	Yellow Sea	17:38	17:39	5:27	8:31
Asia11	30N to 40N	130E to 140E	S. Sea of Japan & S. Coast of Honshu	13:26	14:28	7:21	10:23
Asia12	30N to 40N	140E to 150E	E. Coast of Honshu	16:25	16:27	10:22	11:23
Asia13	20N to 30N	110E to 120E	S. Coast of China	13:35	6:23	9:32	12:37
Asia14	20N to 30N	120E to 130E	East China Sea	11:28	7:22	7:23	10:27
Asia15	20N to 30N	130E to 140E	N. Philippine Sea	9:23	7:19	6:19	7:21
Asia16	10N to 20N	90E to 100E	Andaman Sea	5:23	13:36	9:25	3:20
Asia17	10N to 20N	100E to 110E	Gulf of Thailand & Coast of Vietnam	4:28	1:13	3:21	5:30
Asia18	10N to 20N	110E to 120E	South China Sea	2.5:14	6:19	7:22	4:22
Asia19	10N to 20N	120E to 130E	Philippine Sea	4:15	7:19	7:21	8:22
Asia20	0 to 10N	90E to 100E	W. Straits of Malacca	4:15	4:15	5:16	3:15
Asia21	0 to 10N	100E to 110E	Gulf of Thailand/South China Sea	3:13	4:16	6:20	5:24
Asia22	0 to 10N	110E to 120E	S. South China Sea	3:12	5:16	7:19	6:21
Asia23	0 to 10N	120E to 130E	Sulu/Celebes Seas	4:12	5:15	5:15	5:15
Asia4			Korsakov, Sakhalin, Russia	40%	58%	40%	40%
Asia7			Vladivostok, Russia	32	65	29	12
Asia10			Pusan, Korea	34	59	28	20
Asia13			Hong Kong, China	65	34	25	47
Asia14			Kaohsiung, Taiwan	61	42	71	82

* Because there are so few observations in the Sea of Okhotsk, Areas 1,2, &5 and Areas 3&4 were combined.

6. COMPILATION OF REMOTE SENSING DATA (CHU, TSAY)

The analysis of visibility data reported in the previous section is based on sets of point measurements. In this task, we compile satellite climatologies from the most productive systems. Not only will the standard global climatologies be used, but high-resolution work can also be performed in our regions of interest. In itself, satellite data cannot go far toward investigating the impacts of aerosols on HEL propagation. Clearly, it can define whether or not aerosol particles are small or large in regions of interest, and, hence, the relative efficiency with which particles scatter light in the IR. However, another principal role uses this data in combination with the visibility and model data to derive a consistent picture of HEL propagation. In order to have an overall assessment of extinction, there is a strong need to use satellite remote sensing and mesoscale transport models.

First year goals of Task 4 of this project were to compile aerosol climatologies from various satellite measurements, including MODIS (Moderate Resolution Imaging Spectrometer), SeaWiFS (Sea-viewing Wide Field-of-view Sensor), AVHRR (Advanced Very High Resolution Radiometer), and TOMS (Total Ozone Mapping Spectrometer). From this more extensive data set, spatial patterns of aerosol optical depth were to be generated. Analysis of the data was to occur in the subsequent years. Unlike visibility reports, satellite data are consistently collected over many years. However, as most reported data are column-integrated quantities, it can be difficult to apply satellite data to the marine boundary layer. Table 11 summarizes satellite sensor specifications and derived aerosol properties.

6.1 System Strengths and Weaknesses

The longest records of aerosol optical depth (30+ years) come from the AVHRR and TOMS platforms. Interestingly, neither TOMS nor AVHRR was originally designed to study aerosols. TOMS has the longest record and was the first satellite able to retrieve aerosol properties over land and ocean in the ultraviolet spectrum. Designed for ozone mapping, it was found that by using band math in the 0.34 and 0.38 channels, a qualitative "aerosol index" that was sensitive to absorbing aerosols such as smoke or dust could be generated. Because of the extreme degree of Rayleigh scattering in the ultraviolet, sensitivity increase for higher aerosol altitudes. While useful to the climate community for tracking continental scale dust and smoke events, the aerosol index is difficult to interpret for aerosol particles in the marine boundary layer. Only recently has the TOMS team been able to produce an actual optical depth product. The major uncertainties in TOMS-derived aerosol properties are attributed to the altitude dependence of aerosol particles, and to its large footprint (50×50 km^2). The short wavelengths make extrapolation to the IR very difficult. Lastly, over the last three years, the sensor has begun to degrade and more noise is entering into the product.

With a data set almost as long as TOMS and nearly daily coverage, AVHRR has been the workhorse for long-term aerosol climatologies. Both over water and over land products have been generated. However, the only consistent global product is for over water only. With a spectral channel centered at 0.87 μm (0.725 to 1.10 μm), it is too broad to provide independent spectral information.

Table 11 — Satellite Sensor Specifications and Derived Aerosol Properties

	AVHRR	TOMS	SeaWiFS	MODIS
# Channels	2	2	4	7
Central Wavelengths (μm)	Visible-NIR 0.66, 0.87	Ultraviolet 0.34, 0.38	Visible-NIR 0.44, 0.51 0.67, 0.87	Visible-SWIR 0.47, 0.55, 0.67, 0.87, 1.24, 1.64, 2.1
Sensor Res.	1 km	50 km	1 km	0.25, 0.5, 1 km
Aerosol parameters	τ_a, α	AI, τ_a, α	τ_a, α	τ_a, α, η R_{eff} (ocean only)
Retrieval Res.	1,4 km	50 km	1, 4 km	10 km
Land/Ocean	Ocean	Land /Ocean	Ocean	Land/Ocean (excluding bright surfaces)
Spatial Cov.	Global	Global	Global	Global
Temporal	1983-	1979-	1997-present	2000-present

τ_a: aerosol optical depth; α: Ångstöm exponent; η: fine mode ratio; R_{eff}: effective radius; AI: aerosol index; underscore denotes spectral bands used for over land retrievals
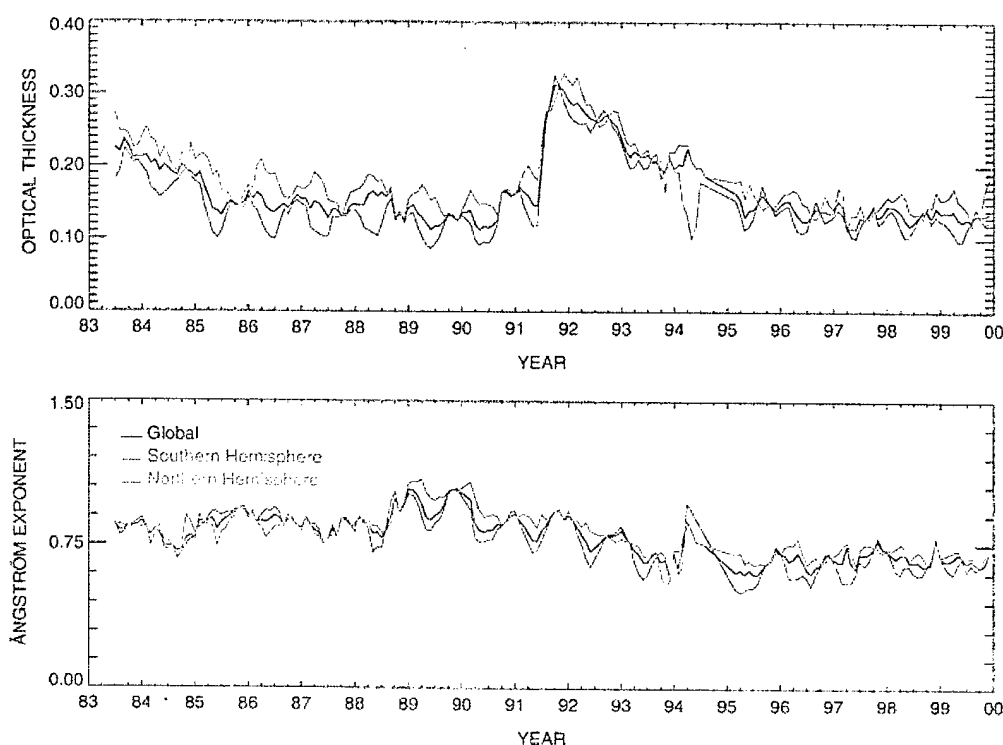
Fig. 7 — Time series of AVHRR GACP τ_a at 0.55 μm (upper panel) and Ångström exponent (lower panel) from 1983-1999. The large increase in τ_a around June 1991 is due to Mt. Pinatubo eruption. (GACP: Global Aerosol Climate Project)

SeaWiFS's mission is primarily targeted to ocean color with aerosol retrievals as a byproduct. With three wavelengths in the visible spectrum, near-real color images can be generated, making SeaWiFS one of the sensors of choice for qualitative regional assessments. The lack of an IR channel makes cloud screening difficult and, consequently, heavy aerosol events such as dust storms can sometimes be masked as cloudy pixels and removed from retrieval processes.

The current flagship sensor for performing aerosol research is MODIS on NASA's Terra and Aqua satellites. MODIS channels from 0.47 to 2.1 μm provide the richest spectral information on aerosols and underlying surfaces. In turn, MODIS is able to derive not only aerosol loading, but also the fraction of fine-mode particle over both land and ocean (except deserts and Sun-glint regions). Aerosol effective radius is also obtained over ocean as a secondary product.

There is no perfect system for performing the HEL propagation assessment. Each satellite sensor has its strengths and weaknesses in aerosol retrieval. While systems such as AVHRR have long records, MODIS produces far superior products. For this assessment we will focus on the global data from AVHRR, TOMS, and MODIS.

6.2 Global and Hemispheric Analysis

The more than 20 years of AVHRR measurements show long records of aerosol properties over ocean (1983-present) (Geogdzhayev et al. 2002; Stowe et al. 1997). No significant annual trend is found at a global scale. The background value of global-averaged aerosol optical depth (τ_a) is approximately 0.14 during quiet periods between volcanic eruptions. Strong seasonal cycles depict maxima in the winter (January-February) and minima in the summer (June-July). The hemispheric means reveal systematically

higher values in Northern Hemisphere than in the Southern Hemisphere. Figure 7 shows the time series of global and hemispheric means from the GACP (Global Aerosol Climatology Project) AVHRR-derived τ_a at 0.55 µm and Ångstöm exponent from 1983 to 1999. Figure 8 shows the seasonal means of spring, summer, autumn, and winter for 1983 to 1999.

Seasonal variation of aerosol events is clearly seen from the 17-year average of AVHRR-derived aerosol optical depths (τ_a). These findings corroborate trends from the visibility reports discussed earlier. In spring, Asian dust outbreaks and biomass burning, as well as wind-blown dust in central Africa, are the most pronounced global features. In summer, dust outbreaks in western Africa and biomass burning in southern Africa, as well as dust storms in central Asia, are the dominant aerosol sources. Note the extremely high values in the Arabian Sea as well. In autumn, the continual biomasses burning in southern Africa and dust outbreaks in western Africa are the most significant. In winter, biomass burning in central Africa is most active. In the south and north polar regions, cloud contamination might have played a critical role in generating high τ_a values, while low τ_a values are found in high-pressure dominant regions because of subsidence.

Figure 9 shows the corresponding Ångström exponent results from the AVHRR time series. Recall, the Ångström exponent is related to the slope of light scattering as a function of wavelength, with lower values indicating larger aerosol particle size, and hence more effect in the near IR. The AVHRR GACP Ångström exponents qualitatively match what is known about global aerosol patterns, as well as with regions of poor visibility. For example, AVHRR depicts low values of the Ångström exponent over dust aerosol dominated regions (such as the coast of North Africa) and high values over biomass burning and urban/industrial pollution outflow regions (such as Asia, Africa, and South America). Because the NOAA Pathfinder data set that we use employs only a single aerosol model, the resulting Ångström exponents are generally confined to the range from 0.6 to 1.2 (a somewhat smaller range than reality). However, any value less than 0.9 indicate areas with a high fraction of coarse mode particles, and hence a more direct relationship between visible and IR wavelengths.
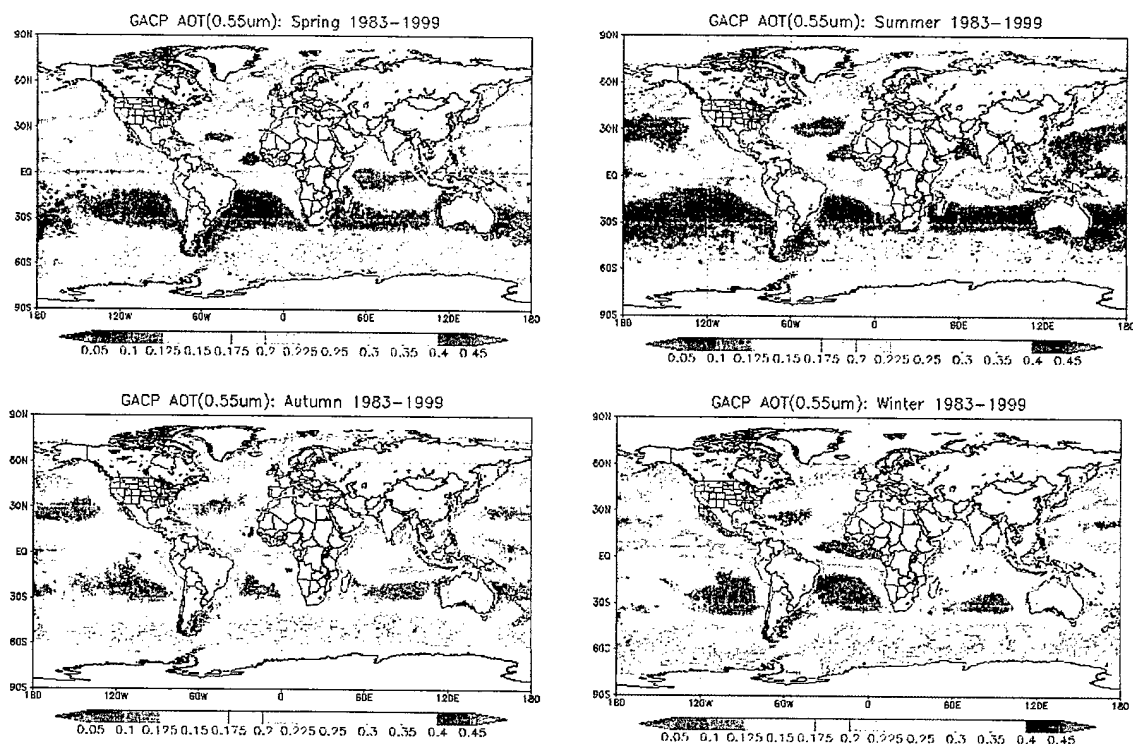
Fig. 8 — Seasonal means of AVHRR GACP τ_a in spring (March-May), summer (June-August), autumn (September-November), and winter (December-February) between 1983 and 1999. (GACP: Global Aerosol Climate Project)
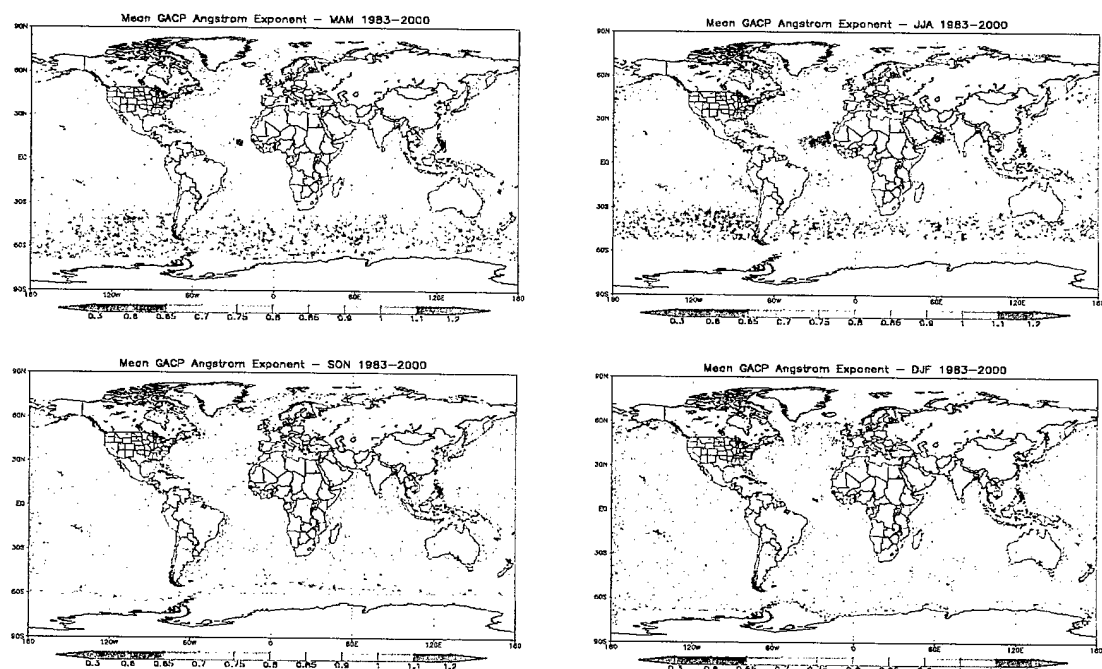

Fig. 9 — Seasonal means of AVHRR GACP Ångström exponent in spring (March-May), summer (June-August), autumn (September-November), and winter (December-February) between 1983 and 1999

TOMS ability to detect absorbing aerosols (dust and smoke) over land using the ratio of 0.34 and 0.38 μm ultraviolet (UV) radiance channels (dark surface in the UV part of spectrum) advances the AVHRR satellite remote sensing time series of aerosols onto land, and into source regions (Hsu et al. 1996; Herman et al. 1997). Figure 10 depicts TOMS seasonal mean aerosol index (AI >0) for dust and biomass burning aerosols from 1983 to 1999. The corresponding TOMS seasonal averages of optical depth presented in Fig. 11 (Torres et al. 1998) shows a mismatch with aerosol index (for example, low τ_a with high AI over Sahara Desert in spring and summer). In addition, a discontinuity is prominent along the coast of central Africa. The different aerosol model used in optical depth retrieval might result in such inconsistencies. Cloud contamination could cause the large τ_a values on the African coast because of TOMS's large footprint. TOMS has captured persistent biomass burning events in central Africa (winter) and dust outbreaks in Saudi Arabia Peninsula (summer) and northern Africa (spring, summer, and autumn). Weak signatures are seen from biomass burning in Southeast Asia and from dust activity in Taklimakan Desert. The uncertainty of aerosol height is believed to be the major factor responsible for the temporal averaging.

MODIS has the shortest time series available, but it clearly has the highest fidelity. MODIS has the ability to provide not only aerosol loading over land ($\Delta\tau_a = \pm 0.05 \pm 0.2\tau_a$) (Chu et al. 2002) and ocean ($\Delta\tau_a = \pm 0.03 \pm 0.05\tau_a$) (Remer et al. 2002) but also the fraction of fine-mode particles, which has drastically broadened our understanding of global aerosols in both source (except deserts) and downwind regions. For comparison, Figs. 12 and 13 show, respectively, the seasonal means of MODIS-derived τ_a and corresponding fine-mode τ_a for spring, summer, autumn, and winter from December 2000 to November 2001.

It is worthwhile to compare the MODIS data in particular with visibility data in Section 5. Examination of the two data sets indicates some differences in the vertical profile of the aerosol particles. From Figs. 12 and 13 it is evident that the greatest impact on HEL wavelengths is expected for the Arabian Sea, followed by North Africa and East Asia. It is noteworthy that the MODIS optical depths are higher in the Arabian Sea than the Persian Gulf, indicating a latitudinal trend opposite to the visibility data. This is in part because over one half of the particles in the region are transported aloft in the free troposphere. Much of the optical depth aloft in the Arabian Sea is due to smoke from Northern India and Pakistan, thus suggesting more dust in the marine boundary layer. It is also worth reminding that aerosol optical depths can only be retrieved in clear sky conditions. Hence, regions with stratus fields, such as those often present off of the Arabian Peninsula, are not depicted in these figures.

A second area of interest is Asia. Spring and summer maximums in optical depth cover most of the Asian east coast. Also noteworthy is the increase of dust in the spring. Even here, however, there is likely to be an under-representation of dust. Because of the high degree of cloud cover in the region, much of the dust and pollution transported into the Sea of Japan or Korean Peninsula probably occurs preferentially during cloudy conditions.
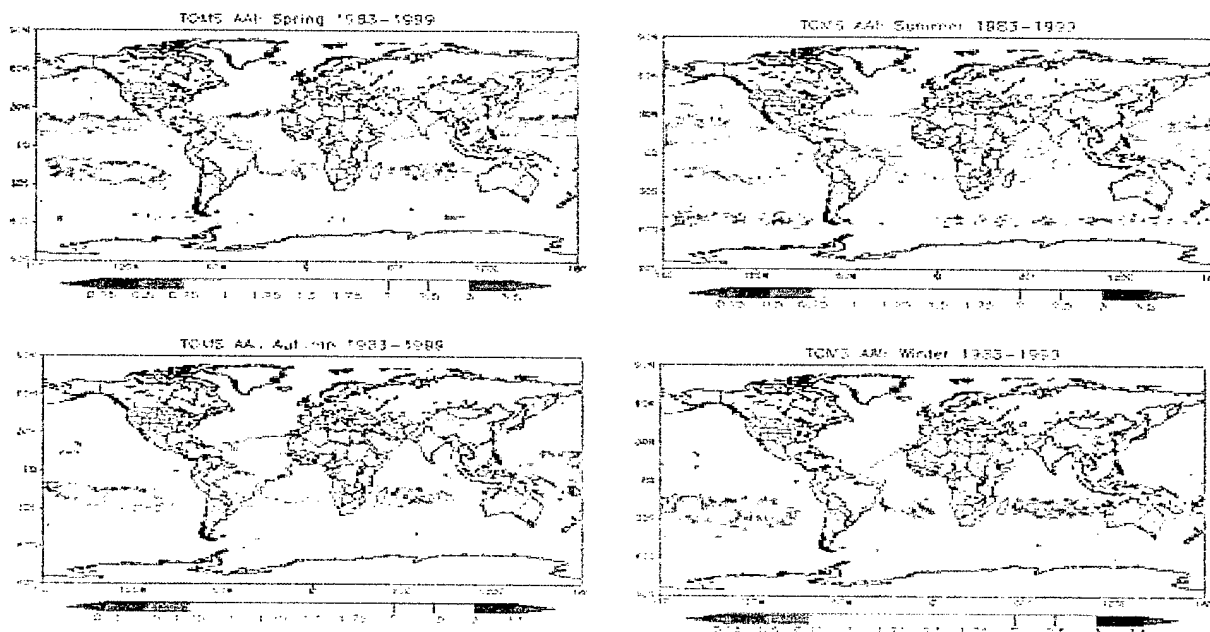
Fig. 10 — Seasonal means of TOMS-derived aerosol index (>0) in winter (December-February), spring (March-May), summer (June-August), and autumn (September-November) between 1983 and 1999.
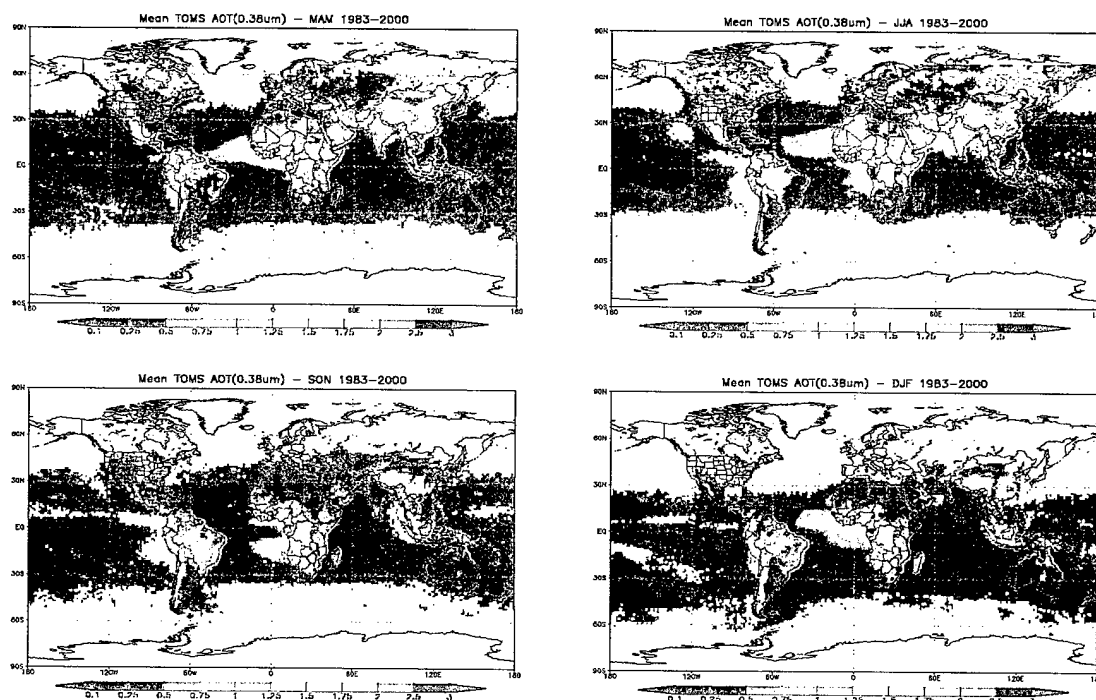

Fig. 11 — Seasonal means of TOMS-derived τ_a (at 0.38 μm) in winter (December-February), spring (March-May), summer (June-August), and autumn (September-November) between 1983 and 1999
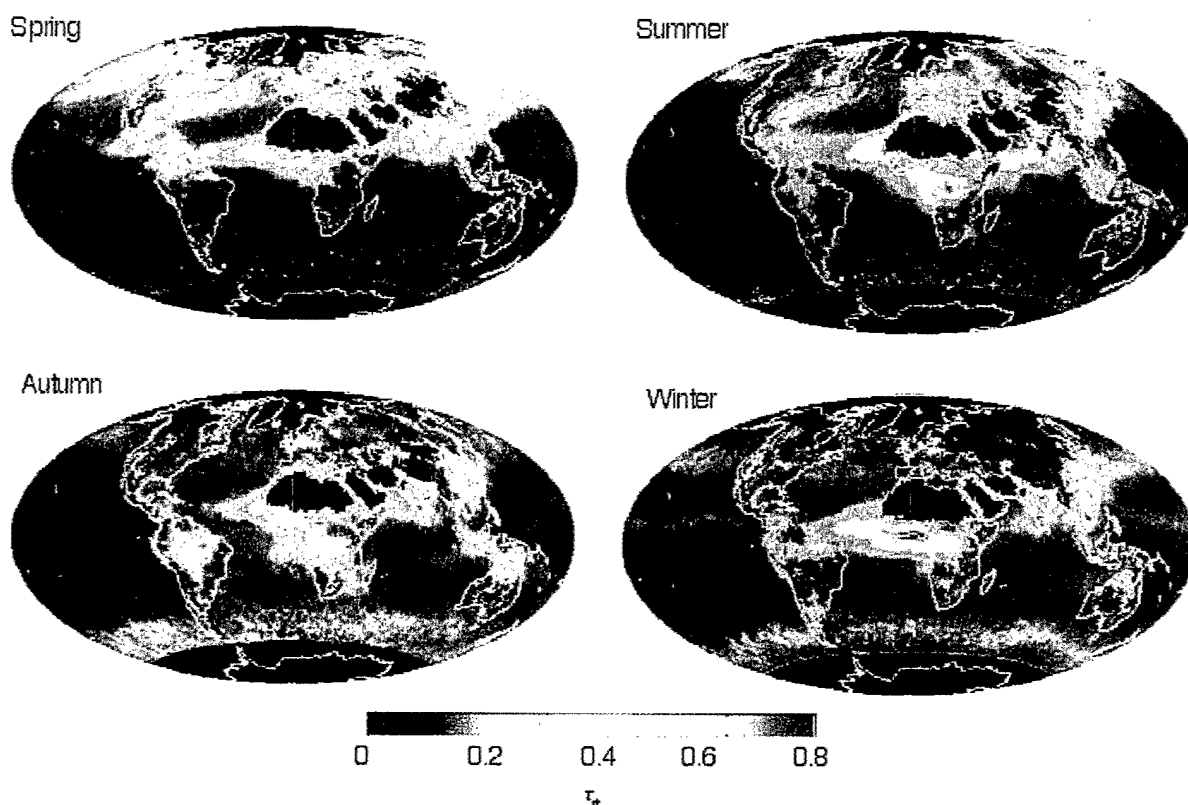
Fig. 12 — Seasonal means of MODIS-derived τ_a for spring (March-May 2001), summer (June-August 2001), autumn (September-November 2001), and winter (December 2000-February 2001)
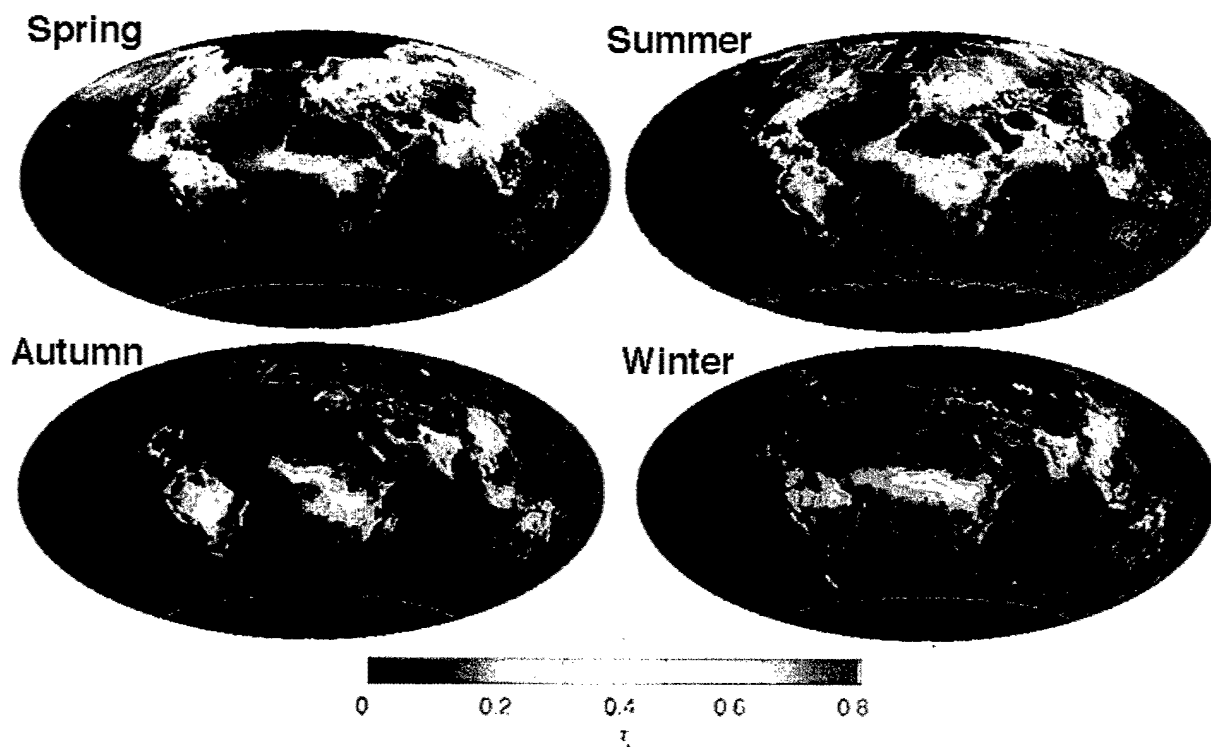

Fig. 13 — Seasonal means of MODIS fine-mode aerosol optical depth for spring (March-May 2001), summer (June-August 2001), autumn (September-November 2001), and winter (December 2000-February 2001)

6.3 Global Intercomparison

In addition to regional comparisons, we have also begun comparisons on a global level. Table 12 summarizes the global and hemispheric averages and standard deviations of AVHRR- (at 0.55 μm over ocean only) and TOMS-derived τ_a (0.38 μm over land and ocean) in different seasons from 1983 to 2000. Figure 14 shows the global and hemispheric averages (and standard deviations) of AVHRR- and TOMS-derived τ_a in different months between 1983 and 2000. The inclusion of the aerosol loading over land increases the global and hemispheric mean τ_a by a factor of 2 to 3. However, a full quantification requires further work on accounting for the wavelength difference.

Table 12 — Global and Hemispheric Averages and Standard Deviations of AVHRR GACP and TOMS Aerosol Optical Depths for Different Seasons from 1983 to 2000

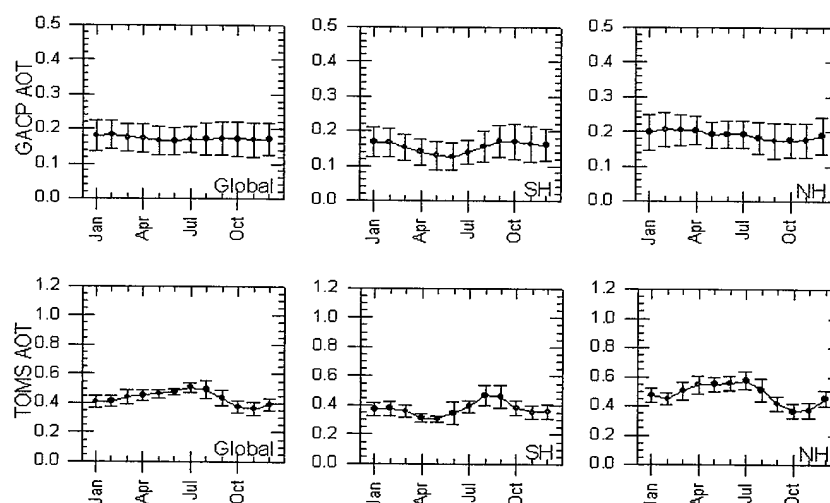|	Season	GACP AOD		TOMS_AOD	
		Mean	STD	Mean	STD
Globe	MAM	0.169	0.065	0.416	0.264
	JJA	0.163	0.081	0.465	0.317
	SON	0.172	0.058	0.372	0.249
	DJF	0.18	0.068	0.365	0.226
SH	MAM	0.146	0.043	0.316	0.14
	JJA	0.138	0.06	0.362	0.243
	SON	0.169	0.053	0.381	0.284
	DJF	0.168	0.05	0.351	0.195
NH	MAM	0.201	0.074	0.5	0.315
	JJA	0.191	0.092	0.53	0.344
	SON	0.176	0.062	0.362	0.206
	DJF	0.197	0.082	0.385	0.262

Fig. 14 — Global and hemispheric averages and standard deviations of AVHRR- and TOMS-derived τ_a in different months between 1983 and 2000

The AVHRR- (1983-2000) and MODIS- (2001) derived τ_a (at 0.55 µm) over ocean show similar monthly variation of global means. Larger differences are only found in regions towards the Poles ($\Delta\tau_a$~0.2-0.3). In the southern hemisphere, MODIS monthly means are consistently lower than AVHRR, while in northern hemisphere MODIS is higher than AVHRR in spring and summer and lower in fall and winter. MODIS-derived Ångström exponents are smaller than those from AVHRR except in May and June. The smaller Ångström exponents (0.4-0.6) between July and December in both hemispheres may be due to the switch of MODIS electronic board (mid-June 2001). Note that AHVRR retrieval Ångström exponents are confined to a narrower range because of the use of the single aerosol model.

Figure 15-18 displays the zonal means of AVHRR- (1983-2000) and MODIS- (2001) derived τ_a for January to December. Three panels (upper: all data; middle: collocated data; lower: # of longitude grids) are plotted for each month. In general, the results of using all data and collocated data are similar. In January and February, MODIS- and AVHRR-derived τ_a values are fairly comparable, with MODIS being slightly higher in the subtropics of the northern hemisphere and slightly lower in the mid-latitude of the southern hemisphere. From March to May, the τ_a values derived from MODIS are significantly higher than those from AVHRR in the northern hemisphere (latitude >10°N) as a result of active Asian dust outbreaks (2001), whereas slightly lower values are seen from MODIS as compared to AVHRR in the southern hemisphere. The high values found in northern hemisphere from June to August are mostly likely caused by air pollution. However, around 50°N in July, cloud contamination may be a contributing factor to the large τ_a values (~0.4 for all data and 0.6 for collocated data). Comparable results are also found in September to December except in the tropics (AVHRR>MODIS) and around the South Pole (MODIS>AVHRR).

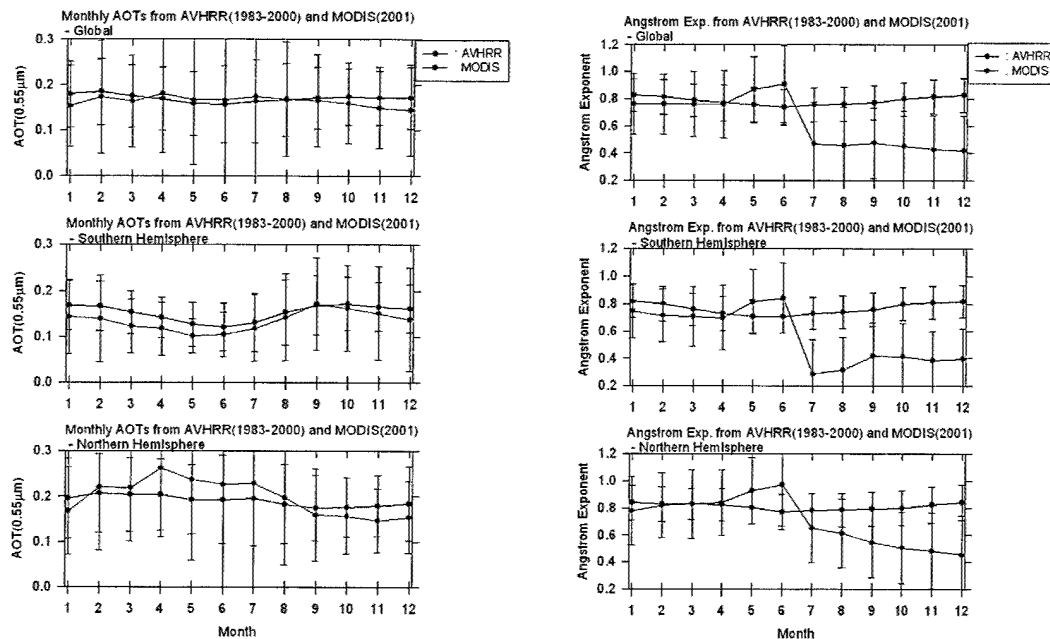Fig. 15- Global and hemispheric averages and standard deviations of AVHRR- and TOMS-derived τ_a and Ångström exponents in different months between 1983 and 2000.
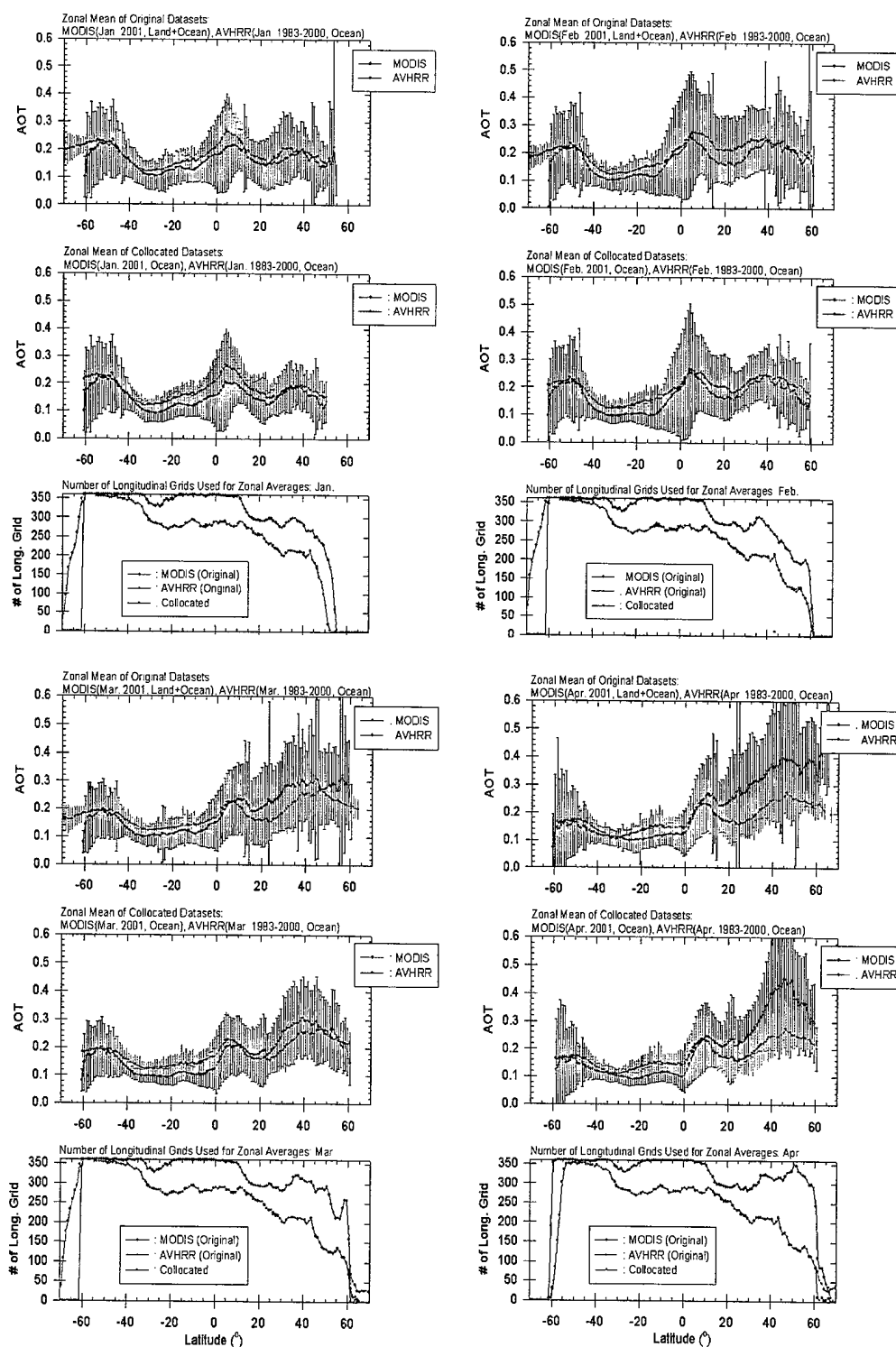
Fig. 16 - Monthly averages and standard deviations of AVHRR- and MODIS -derived τ_a from 1983 to 2000: January through April
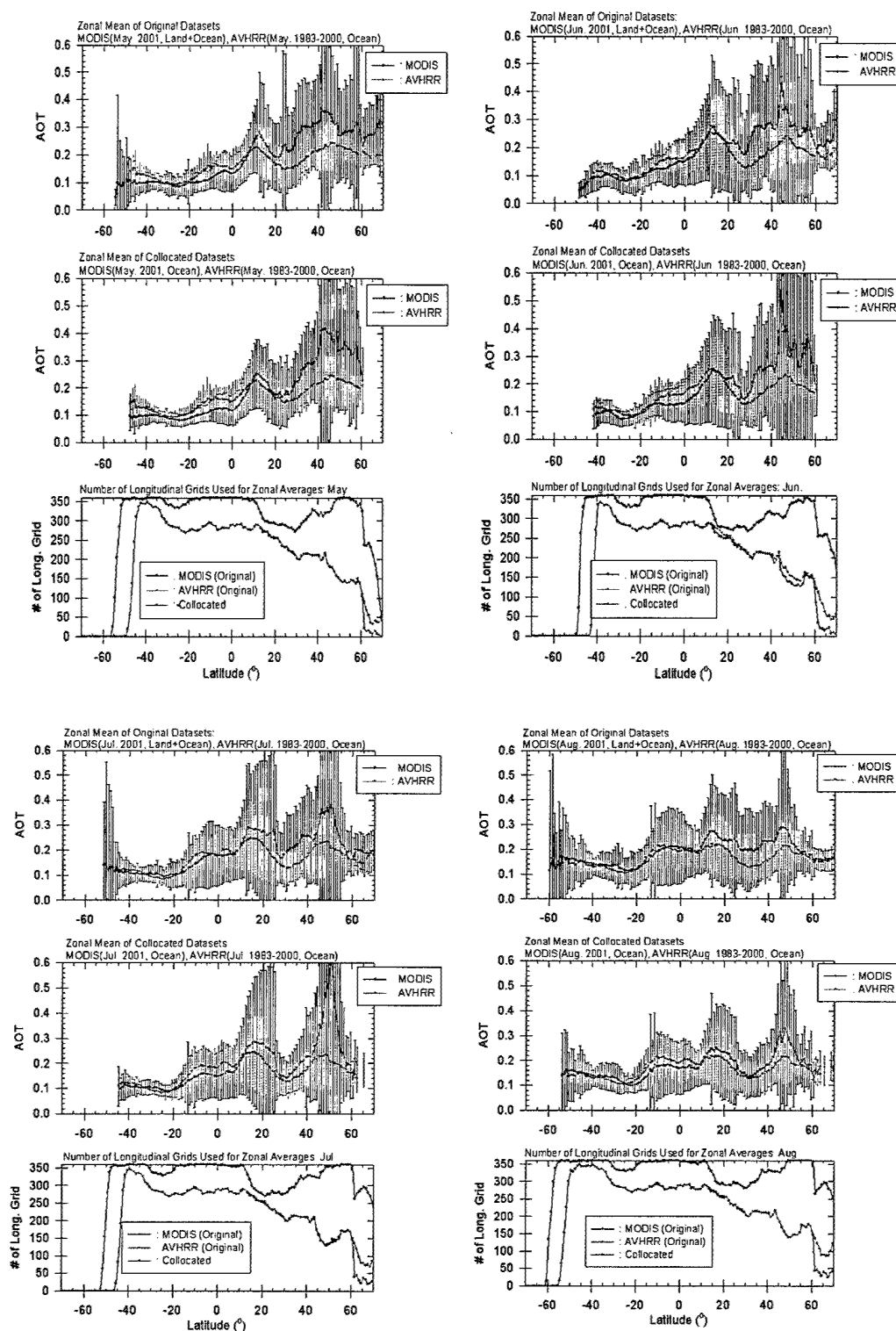
Fig. 17 - Monthly averages and standard deviations of AVHRR- and MODIS -derived τ_a from 1983: May through August
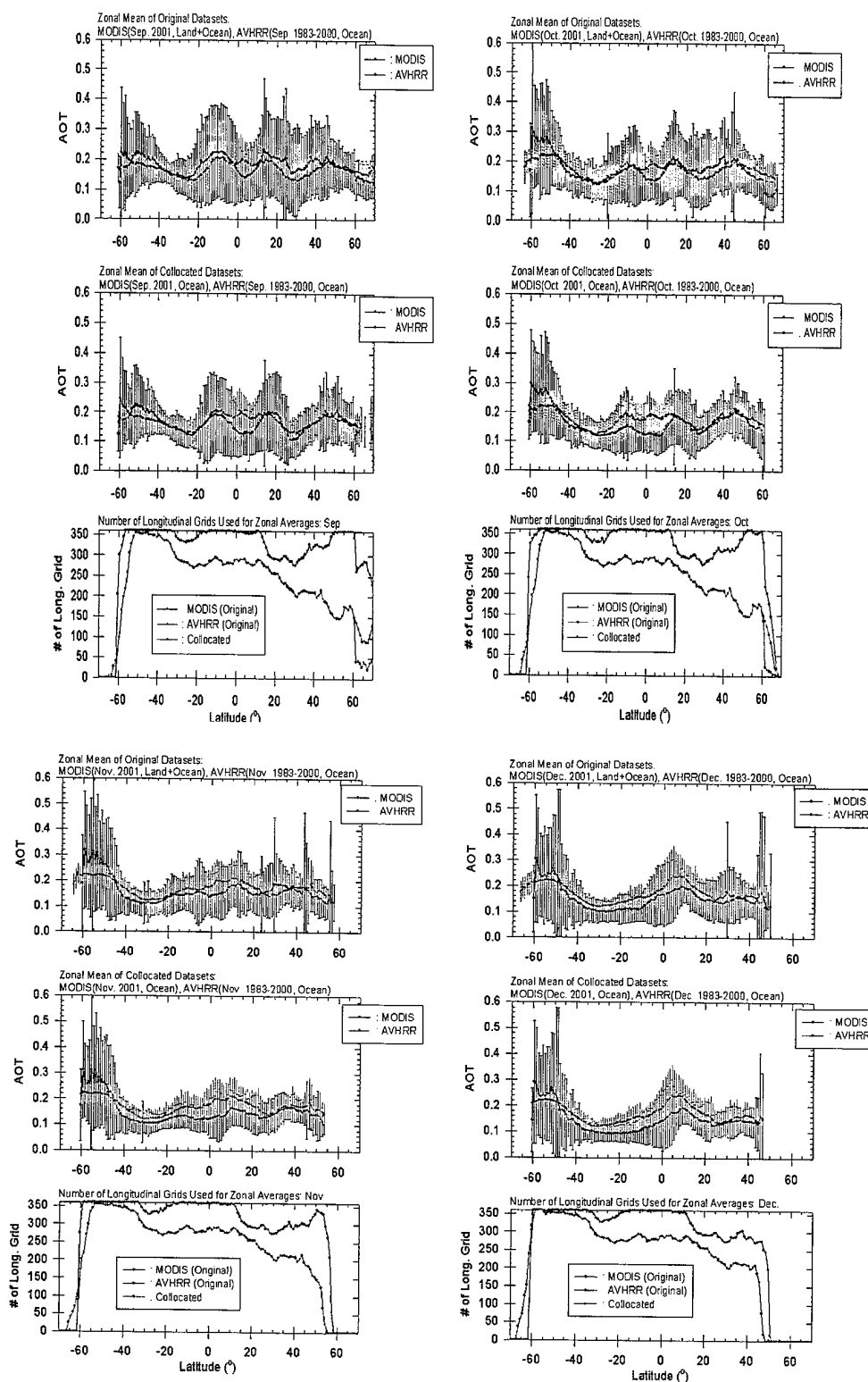
Fig. 18 - Monthly averages and standard deviations of AVHRR- and MODIS -derived τ_a from 1983: September through December

6.4 Regional Intercomparisons

As part of Task 4, regional studies in areas of interest were to be made. Figure 19 shows preliminary areas where summery statistics were to be generated. The selected regions are based upon (1) high frequency of aerosol events (e.g., dust outbreaks in Saharan desert and western Africa), (2) high aerosol loading (e.g., seasonal biomass burning events in SE Asia, S. Africa and S. America), (3) low aerosol loading (e.g., pristine remote oceans), and (4) occurrence of transient aerosols (e.g., dust/smoke/pollution outflow regions

The goals of year one of this project were to gather the required satellite data for a detailed analysis to be made in years two and three. For the purposes of this preliminary report, three areas are discussed. These are regions 7 (Arabian Sea), 14 (Sea of Japan), and 18 (South China Sea). The purpose of this is to not only to convey information in these interesting theaters, but also to demonstrate the inherent benefits and uncertainties in doing such an analysis.

Figure 20 shows the monthly mean τ_a and Ångström exponent of AVHRR (1983-2000) and MODIS (2001). Overall MODIS-derived τ_a values are larger than those obtained from AVHRR, especially in active dust seasons in regions 7 (July) and 14 (March-May) and in the biomass burning season in region 18 (April). Note that these are not real one-to-one comparisons. AVHRR data are used as aerosol climatology. AVHRR 2001 data are of bad quality, while MODIS 2001 data is good. MODIS 2000 data used an earlier version of the MODIS aerosol algorithm (V2), and thus cannot be used to compare with AVHRR 2000 data. The latest MODIS data version (V4) is currently going into production (April 2003). Still these results could reflect temporal deviations, e.g., the dust outbreak is stronger in 2001
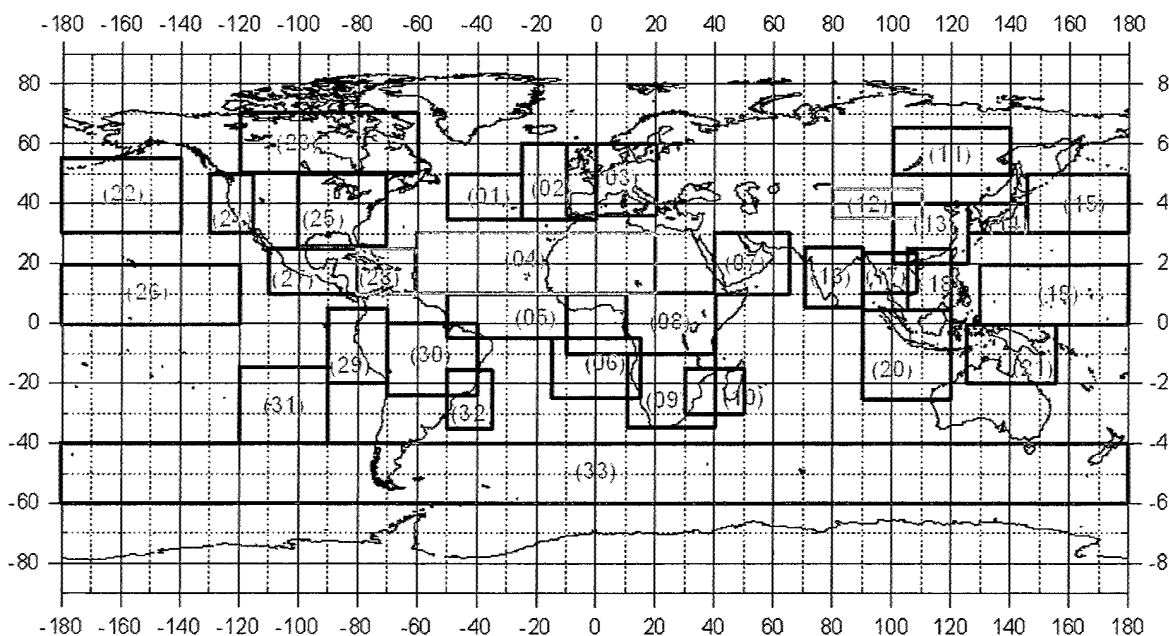

Fig. 19 - Regions selected for building statistics of aerosol properties for dust (yellow), smoke (black) and sulfate (blue), sea salt (pink), and mixed (red) aerosols.

compared to the climatology. In many ways, the drought-induced loss of vegetated surface seems to correlate well with intensified dust outbreaks in western and northern China and in south Asia from 1998 to 2002. In terms of Ångström exponent, MODIS shows generally larger variations compared to AVHRR. Similar conclusions can be drawn from the histograms of τ_a (see Figure 21).
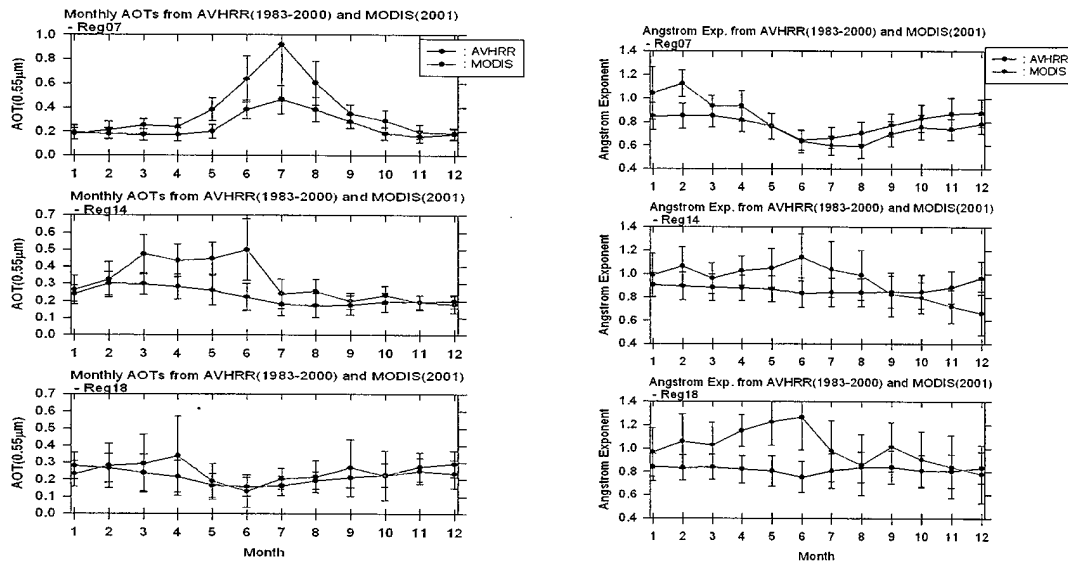

Fig. 20 — Month mean τ_a and Ångstrom exponent of AVHRR (1983-2000) and MODIS (2001) over ocean only. Region 7 = Arabian Sea and Persian Gulf; Region 14 = Sea of Japan; Region 18 = South China Sea
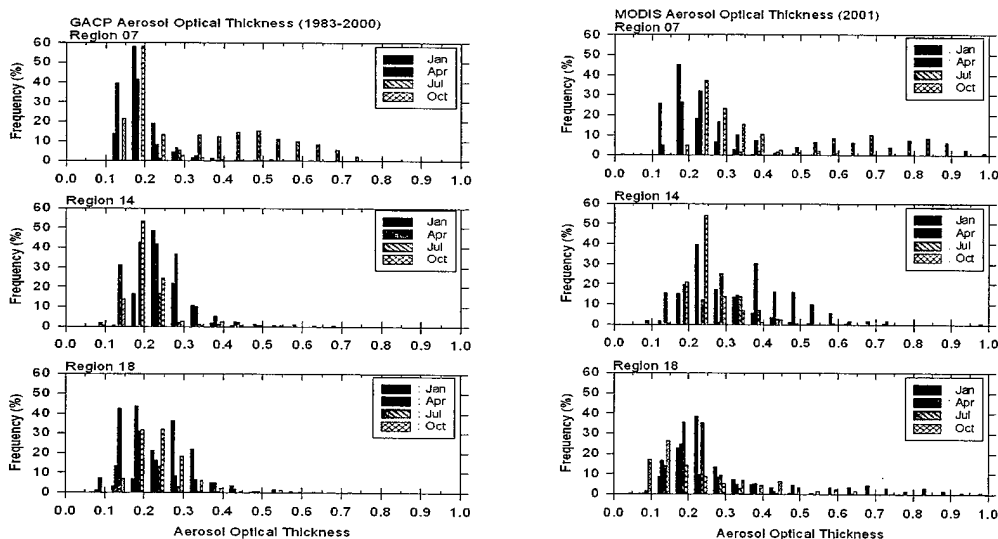

Fig. 21 — Histogram of AVHRR derived optical depth (1983-2000) and MODIS derived optical depth (2001)

6.5. Issues with Satellite Data, HEL Impacts and Future Work

The goals for the first year of this project were to collect global satellite data and process it into a form useful for future studies on HEL propagation. Preliminary results are encouraging. However, before the data can be fully utilized, several more steps must be taken. First, cloud contamination is a continuing issue in all data sets and is often regional in nature (e.g., polar regions for MODIS retrievals; coastal zones for TOMS retrievals). A second issue is the need for more intercomparisons between AVHRR and TOMS (at 0.55 µm, not at 0.38 µm) for 1983-2000, especially to determine whether the wavelength dependence of data can be utilized. Lastly, spot measurement intercomparisons between MODIS (V4) and AVHRR for January to December 2000, and between MODIS (V4) and TOMS (at 0.55 µm, not 0.38 µm) for January to December 2001 need to be performed. As dust particle asphericity can bias satellite retrievals, more validation work during this intercomparison is necessary in Africa, SW Asia, and East Asia.

7. MODELING THE ENVIRONMENT

Ultimately a HEL propagation assessment must be unified within a propagation model. Such a model requires two elements. First, global and meso-scale models are required to estimate large-scale aerosol transport. Second, a near-surface model is required over the ocean to combine aerosol effects with those of water vapor, bulk refraction, scintillation, and thermal blooming. In this section we discuss progress on these latter issues. Section 7.1 was taken primarily from the TNO Netherlands Report "Marine Aerosols: The Near Surface Component" by R.J. Decae and A.M.J. van Eijk (SPAWAR Systems Center Contract through ONR London N00044-02-1-0746). This is the combined report for this HEL research, as well as for the independently funded Advanced Navy Aerosol Model (ANAM) research. Relevant portion are reprinted with significant augmentation in regards to HEL issues. Requests for the full report should be directed to Dr. A.M.J. van Eijk (affiliation in Appendix A).

7.1 The Near Surface Marine Environment (Decae, van Eijk, Reid)

Atmospheric extinction, turbulence and refractivity at levels from sea surface to about 30 m need to be considered to describe the relevant phenomena, and to assess the effects of the atmosphere on the detection of low-altitude point targets at long ranges. Extinction due to absorption and scattering by aerosols and molecular species reduces the contrast ratio of the target to the natural background. Small changes in the refractive index due to turbulent fluctuations of the airflow, the air temperature and the humidity result in scintillation and in beam wander. Variations of the mean refractive index with height due to atmospheric stratification cause ray bending, i.e. super-refraction or sub-refraction and mirage effects.

Abundant literature exists on each of these phenomena. The interested reader is referred to Zuev (1974), McCartney (1976) and Thomas and Duncan (1993) for transmission phenomena. Turbulence is discussed by Hufnagel (1978), Panofsky and Dutton (1984) and Beland (1993). Refraction effects are discussed by Pernter and Exner (1922), Skolnik (1962), Batten (1973) and Kravtsov and Orlov (1990).

However, relatively few of these publications focus on the particular domain of LR-IRST or HEL applications. DeLeeuw et al. (1995) present a general description of atmospheric phenomena that affect LR-IRST systems. The maximum detection ranges considered in those days were on the order of 10 to 15 km. However, present day technology allows for detection ranges of 20 to 25 km, depending on atmospheric conditions. This, in addition to the fact that part of the propagation path may be very close to

the sea surface where extinction and refraction effects differ from those at higher levels, requires a revisit of the description of atmospheric phenomena.

In recent years, the interest in aerosols has grown appreciably as the scientific community addresses questions related to the local and global climate, visibility and the development of electro-optical surveillance systems. Since the oceans cover 70% of the Earth, considerable efforts have been made to characterise and understand the behaviour of marine aerosols. A problem here exists, since the concentration of marine aerosol in the atmosphere results from a large number of coupled dynamic and physical processes. These are further discussed in the TNO report. However, there are some specific mechanistic issues that should be considered when HEL propagation is assessed.

Several details of the production mechanisms of sea spray are poorly understood. This in turn makes it difficult to model precisely the amount of droplets that is generated from the surface (the so-called source function). In addition, measurements of the aerosol concentration very close to the surface are difficult to make, even in the laboratory under controlled conditions. As a result, the source function for sea spray is not very well known and estimates vary up to several orders of magnitude as shown by Andreas (1998) and further discussed by Reid et al. (2001).

After their generation, the saline droplets find themselves in the turbulent airflow close to the surface. This flow is highly fluctuating due to the presence of the waves and necessitates a detailed and elaborate description. The turbulent airflow above waves has been the subject of numerous studies, starting with Miles (1957) (see Belcher and Hunt (1998) for a review). The droplets are transported out of their production zone by turbulent diffusion and convective flow, which are counterbalanced by inertial resistance of the particles and gravitational forces. While the sea-spray droplets are airborne, they interact with the scalar fields of temperature and humidity by exchanges of heat and moisture. In this manner, the droplets influence the humidity and sensible heat fluxes, and thereby may have an impact on the coupling between ocean and atmosphere. It has been estimated (see Wu (1974) and a review by Andreas et al. (1995)) that the water vapor flux due to the evaporation of sea spray may become comparable to that from direct evaporation at the sea surface for wind speeds of around 15 m/s.

Relative to other aerosol species, these mechanistic issues for sea salt described above can significantly complicate HEL propagation assessments. Most importantly, as the ocean surface is a source as well as a sink for salt particles, the vertical distribution of extinction varies considerably as a function of wind speed and stability. Gradients are particularly strong in the lowest 10 m where sea skimming missiles often travel. During high wind events with offshore flow, the latent heart flux due to salt particles will result in higher humidity in coastal waters.

The assessment of the effects of sea salt and these near surface phenomenon was delegated in Task 5 of this project. Such work has historically been tackled by an experimental approach, followed by statistical modeling. Examples of such studies include DeLeeuw et al. (1995) and DeLeeuw et al. (1996). With the increase in our knowledge of the underlying physics, numerical or process modeling has recently become possible.

In parallel with the experimental efforts, models were developed to assess the marine aerosol concentration as function of the meteorological conditions. The commonly used Navy Aerosol Model (Gathman 1983), which predicted the marine aerosol concentration at ship's deck height for open ocean

conditions, is still the most commonly used marine aerosol model in the DoD. The original NAM has been updated on the basis of new experimental (DeLeeuw 1986a; Hughes 1987) and theoretical (Gerber 1985; Gathman 1989) evidence, and is presently included in the widely used USAF MODTRAN transmission code.

Up to this study, all aerosol propagation studies for HEL have used NAM and hence it is worth discussing here. The NAM describes the aerosol size distribution at a height of 10 m by a superposition of three lognormal curves ("modes"). Each mode is characterised by a lognormal curve of the number distribution defined by a width (assumed constant geometric standard deviation of 2), a center diameter and an amplitude. The center diameters of the modes are nominally 0.06, 0.48 and 4.0 μm at 80 RH (but are adjusted as function of the relative humidity). The corresponding volume median diameters (VMD) are roughly 0.25, 2, and 16 μm. The largest or third mode (16 μm volume VMD) is modelled to be from instantaneous production of, say, spume, and its amplitude is determined by the instantaneous wind speed. The second mode (2 μm VMD) consists of marine aerosols that have spent some time in the atmosphere ("aged" marine mode). Since these particles have been produced elsewhere and transported to their present location, the amplitude of the second mode is defined by a regression against the average 24 hr wind speed at the receptor site. Finally, the first mode (0.25 μm VMD) consists of fine particles presumed continental in origin. Its amplitude is determined by the so-called "air mass parameter", which in turn is related to the visibility at 0.55 μm. Depending on the value of the air mass parameter, the first mode is separated in a hygroscopic (center radius adjusted according to humidity) and a nonhygroscopic (fixed center radius of 0.03 μm) part. This last component is referred to as the 0th mode.

NAM and the later version NOVAM (Gathman et al. 1989) have been widely used by DoD agencies to estimate EO effects of marine aerosol particles. However, what must be recognized is that the NAM family of models is designed for remote open ocean conditions and is based on a late 1970/1980-era dataset. It was also confined by very limited computational power. Consequently, NAM-like models are considered outdated and suffer from fundamental errors. Most significantly, the placements of the aerosol modes are grossly in error. As shown by Porter and Clarke (1997) and Reid et al. (2001), the NAM modes are considered outliers when compared to measurements by other investigators. Physically, sea salt does in fact have three modes. The fine mode VMD (0.25 μm) is probably a bit small (should be ~0.3) for more polluted marine conditions, and the geometric standard deviation is too small (should be ~1.7 instead of 2). For the purposes of HEL propagation, however, this is irrelevant as long as it is understood that the AMP should be given a value of 0 (no continental influence) and pollution should be dealt with separately. The background marine environment does have it own fine mode component from sea salt and DMS oxidation to sulfate, but its influence on IR propagation is fairly small.

More important, however, is the second mode modelled with a VMD of 2 μm. This size is probably small by a factor of two or three. Best estimates for such a mode place it in the 4 to 7 μm range. Physically, the mode is produced by the bursting bubbles of whitecaps. Particles in this size range can be transported long distances, and NAM tries to cope with this issue by relating its amplitude to the average 24 hr wind speed at the *receptor site.* However, winds at a receptor site are a poor substitute for a true air mass history, as air passes through features with high winds such as fronts or even cyclone remnants. There are several important impacts of these issues on HEL propagation assessments using NAM-like models. First, the mislocation of the mode introduces erroneous wavelength dependence in light scattering in the near IR (it should be more or less wavelength independent in the near and mid-IR).

Second, the use of a mean 24-hr wind speed causes a great deal of scatter and likely underestimates extinction.

The 3rd mode of NAM is the only mode that lends itself to regression type modeling. Placed at a VMD of 16 µm, this mode accounts for the largest sea spray particles that are for the most part generated through spume production. As these particles are large, their atmospheric lifetime is typically on the order of hours. Hence, defining their amplitude by current wind speed is legitimate. However, the 3rd mode in NAM and NOVAM is also placed at too small a size, resulting in under-prediction of atmospheric extinction.

In an effort to correct for the largest particles, the Advanced Navy Aerosol Model (ANAM) was developed to extend the NAM aerosol concentration from 10 meters down to the wave surface. The initial development of the ANAM focuses on the behaviour of relatively large (radius in excess of 5 µm) aerosols. The rationale for this is twofold: first, DeLeeuw et al. (1989) have suggested that the NAM underestimates the concentration of these larger aerosols resulting in an estimate of the (IR) extinction that is too low (see, e.g., DeLeeuw et al. 1986). Secondly, turbulence is less efficient in transporting these heavy aerosols upward from the sea surface, which will (theoretically) result in steeper vertical concentration gradients (see, e.g., Fairall et al. 1982). The aim of the ANAM development is to extend the NAM by a height- and wind speed-dependent 4th mode with a VMD of 25 µm. While the erroneous 3rd mode is still in ANAM, its impact relative to the 4th mode is very small. In a later phase of the development, the necessity of introducing height dependence in the other (NAM) modes will be assessed.

Like its predecessor, NAM, the ANAM was developed by establishing empirical relations between the aerosol concentration and meteorological parameters (Gathman et al. 1998). Unfortunately, measurements of vertical aerosol concentrations between the wave surface and deck height are sparse and almost exclusively limited to the Rotorod technique deployed by TNO-FEL (DeLeeuw 1986). Even when data are available, the uncertainty in the data is often considerable due to the difficulties encountered in making near-surface measurements. To further complicate the problem, the relatively simple relationships that exist at deck level between, e.g., wind speed and aerosol concentration, become more complex closer to the surface due to the influence of the waves.

In view of these complications, the further development of the ANAM requires a full analysis of all available near-surface aerosol data. However, even with a large data set questions remain as to whether a purely empirical ANAM may be accurate enough to reproduce all variations in the near-surface aerosol transmission. Therefore, numerical or physical models that capture the complex interplay of physical processes at the air-sea interface must support the ANAM development. Such models may be used to reveal trends that are currently hidden in the data (due to the limited amount of data or relatively large uncertainties), or to extend the ANAM to meteorological conditions not covered by the database.

For this HEL project, ANAM was to be employed to generate open ocean climatology for extinction in IR wavelengths. However, first ANAM's performance needed to be compared to first principle models. For this purpose, work was performed on developing the SeaCluse model. The French-Dutch SeaCluse model aims at a description of all relevant processes. To achieve this goal, compromises have initially been made as to the level of detail of the some of the processes. The model is the marine version of the CLUSE (Couche Limite Unidimensionelle Stationnaire d'Embruns) model, which aimed at a description of the turbulent transport of evaporating droplets and their interactions with the scalar fields of

temperature and humidity in a laboratory situation (Rouault et al. 1991). The CLUSE model was adapted to oceanic conditions by the introduction of a module to describe the airflow over a wave surface, and a module for the evaporation of salt-water droplets. The airflow module has been tested with non-evaporating droplets and the results have been reported by (Mestayer et al. 1996). The results of the first simulations for evaporating droplets have been reported by (Van Eijk et al. 2001).

The development of the SeaCluse model is not finished. A series of sensitivity analyses is being performed to identify those modules in the model that are most critical to the assessment of the aerosol concentration in the marine surface layer. On the basis of these results, certain modules are to be upgraded to provide a better description (Navarro et al. 2001). Comparison with experimental data has shown that the SeaCluse model now provides reasonable estimates of the aerosol concentration and vertical gradients in the marine surface layer. At the same time, the SeaCluse model is being exploited to provide guidelines for the further development of ANAM (Van Eijk et al. 2002) and the modeling of refraction effects (Navarro et al. 2001).

7.2 Global and Meso-scale Modeling of Severe Visibility Reducing Events (Westphal, Liu)

Ultimately, any EO assessment needs to be formed around a full meteorological model (preferably operational). The Naval Research Laboratory (NRL) in Monterey, CA, has developed near-operational systems for forecasting the three-dimensional distribution of dust, sulfate, and smoke aerosols for the globe and regionally. The global and regional models are called the NRL Aerosol Analysis and Prediction System (NAAPS) and the Coupled Ocean-Atmosphere Mesoscale Prediction System (COAMPS^{TM}), respectively. The purpose of Task 6 of this project was to use NAAPS and COAMPS^{TM} to generate specific propagation scenarios and provide information on the vertical distribution of aerosol particles.

NAAPS is a real-time operational system for forecasting the global distribution of tropospheric sulfate, dust, and smoke aerosols. NAAPS is a modified form of a hemispheric model of sulfate aerosols developed by Christensen (1997). NAAPS uses global meteorological fields from NOGAPS (Hogan and Rosmond 1991; Hogan and Brody 1991) on a 1 X 1 degree grid, at 6-hour intervals and 24 vertical levels reaching 100 mb. NAAPS is currently run globally twice daily and generates 5-day forecasts (see example output at http://www.nrlmry.navy.mil/aerosol).

The model has several highly desirable qualities for studies of the EO propagation. The global scale of the model avoids the problems associated with regional studies, such as boundary conditions, and allows inter-continental transport and mixing. The model is driven with the analyzed dynamical fields from NOGAPS (e.g. *real* weather). This aspect allows direct comparison of the simulated aerosol fields with surface, airborne, and satellite observations. The model is operated in real-time, which allows timely evaluation of the model and notification to downwind-instrumented sites of approaching aerosol events. The model allows multiple species and can easily be expanded to include more species as needs arise.

Currently there are three aerosol species in NAAPS. Dust emission occurs whenever the friction velocity exceeds a threshold value while the surface moisture is less than 0.3. The threshold friction velocity is set to infinity except in known dust-emission areas where it is 60 cm/s (Westphal et al. 1988). These areas are currently defined as areas covered by the eight erodible land-use types used in the USGS Land Cover Characteristics Database with modifications based on climatology from the Total Ozone Mapping Spectrometer (TOMS) Aerosol Index (AI) over the Sahara and Southwest Asia. Global smoke emissions are based on real-time detection of fires by the Wildfire-ABBA (Prins et al. 1998) and

Moderate-resolution Imaging Spectrometer (MODIS) fire products. Emission factors for the USGS land cover types are based on data collected from various geographic regions such as mid-latitude forest, tropical forest, and grass/pasture (Radke et al. 1991; Hobbs et al. 1997; Le Canut et al. 1997; Reid and Hobbs 1998). The sulfur dioxide emission is based on the GEIA inventory, version 1A, for the year 1985 with a seasonal variation and two-level vertical distribution (Benkovitz 1996). Natural emissions of DMS are immediately converted to 95% sulfur dioxide and 5% sulfate. The gas-phase chemistry is described by a simple linear reaction rate that depends on the time of year and latitude.

While NAAPS is run off line with support of NOGAPS data, the regional aerosol model is imbedded within the COAMPS™ Mesoscale model, i.e. it is an in-line module of the prediction system, using the model's exact meteorological fields at each time step and at each grid point for each grid mesh, instead of using history files. This method allows more accurate simulation of diurnally driven processes such as boundary layer mixing or fast changing conditions such as frontal passages.

Once an aerosol is injected into COAMPS™, it is transported using a 5th-order accurate flux-form advection scheme in both horizontal and vertical. The particles are mixed vertically using the turbulent kinetic energy predicted by COAMPS™. The model produces 3-day forecasts of mass concentration, mass load, extinction coefficient and optical depth.

As part of Task 6, aerosol species were to be integrated into COAMPS™ for use in HEL specific simulations. In year one of this program, dust was integrated and tested. Biomass burning smoke and sea salt were also integrated (although not tested). Currently COAMPS™ produces a 3-day forecast of dust for Southwest Asia starting at the 00Z analysis time, followed by a 12-hour update cycle at 12Z each day. At these synoptic times the dynamical fields undergo data-assimilation whereas the dust is continuously simulated throughout time. The model has three nested grids of 9, 27 and 81-km with the domains centered in Iraq, shown below on the right. It is important that the 81-km mesh covers the eastern half of the Sahara Desert since dust from this desert is often transported to SW Asia and beyond. The model allows the dust from the 81-km mesh to pass into the 27-km mesh, and likewise from the 27-km mesh into the 9-km mesh. These are shown in Fig. 22.

Examples of the capabilities of both NAAPS and COAMPS™ models are the forecasts in support of Operation Iraqi Freedom. Consider the dust storm of March 25-27, 2003 (Fig. 23). This event started with strong SW winds over Saudi Arabia and Iraq on March 25, followed by a strong frontal passage with NW winds behind it on March 26, and then strong W winds on March 26 and 27. All three wind regimes lifted dust. Over the period of March 20-22, NAAPS provided the 5-day forecasts of the three wind regimes. An example is shown in the top-left panel of Fig. 23, which shows a time-height sectional plot of the forecasted dust concentration at Kuwait for 19-26 March 2003. An earlier dust storm is apparent on the 19th and 20th. The storm of interest is seen beginning on the 25th and intensifying on the 27th, as was observed. Variations in dust vertical distribution were also observed.

On March 23, the 3-day COAMPS™ forecasts started covering the event. It too forecasted the wind regimes and, furthermore, captured the detailed structure of the dust front passage, in agreement with surface observations. The forecasted dust front is shown in Fig. 23 on the upper right, which represents the surface dust concentration at 06Z on March 26, 2003. The front is apparent as the feature aligned NNE-SSW through the disputed zone east of Kuwait. This is the first simulation and forecast ever of a dust front showing this detailed structure.

Smoke is also included in COAMPS™ for the SW Asia runs. It was anticipated that Iraqi forces would ignite significant portion of their oil wells in the south and northeastern parts of their country. In preparation for this we included oil well emissions in the NRL Aerosol Analysis and Prediction System (NAAPS) aerosol forecast model as well as a special smoke aerosol component in COAMPS™. The oil
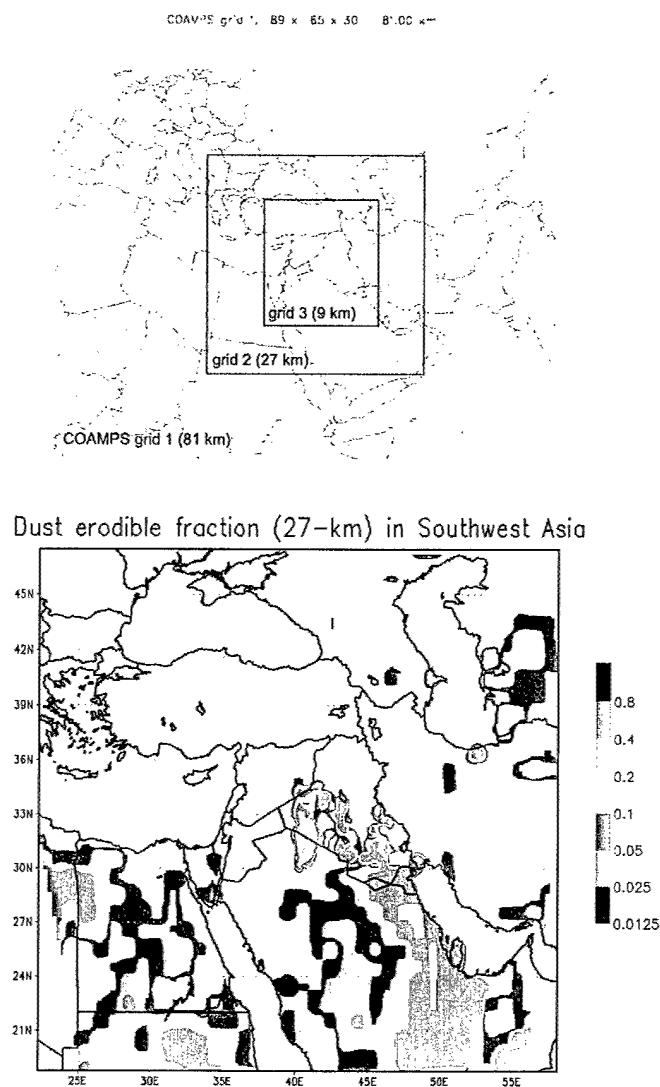
Fig. 22 — Current domains and dust erodibility index for COAMPS of the Southwest Asian theater

smoke component from these two models drew heavily from the code currently used to forecast smoke coverage and visibility effects from biomass burning such as the burning of the rain forests and savannas of South America and Africa.

While the Iraqi oil field survived the operation relatively well, it did provide a good test of the system. Approximately 11 wells were set alight as well as several large oil pits around the city of Baghdad. The lower image in Fig. 23 shows the vertically integrated smoke concentration for the weather on March 23rd. This is an example run where a source was placed in each of the major Iraqi fields. Satellite analysis of the few wells that did burn verified the model predictions.

Currently there are plans to develop climatologies from NAAPS and COAMPS[TM] that will aid further HEL research. A three-year rerun of NAAPS (2000-2002) is underway which will be used to develop a baseline for dust storm frequency and dust vertical distribution. A smoke climatology will be developed as well. COAMPS[TM] will also be run for a set of case studies in Africa, SW Asia, and East Asia.

NAAPS Dust (ug-m**3)
at kuwait (29.22,-47.98) for 2003031900_2003032600

Dust surface concen (mg/m^3) 48h fcst valid at 00Z26MAR2003
COAMPS starting from 00Z24MAR2003 grid 9-km

Iraq oil smoke load (mg/m^2) 06h fcst valid at 06Z23MAR2003
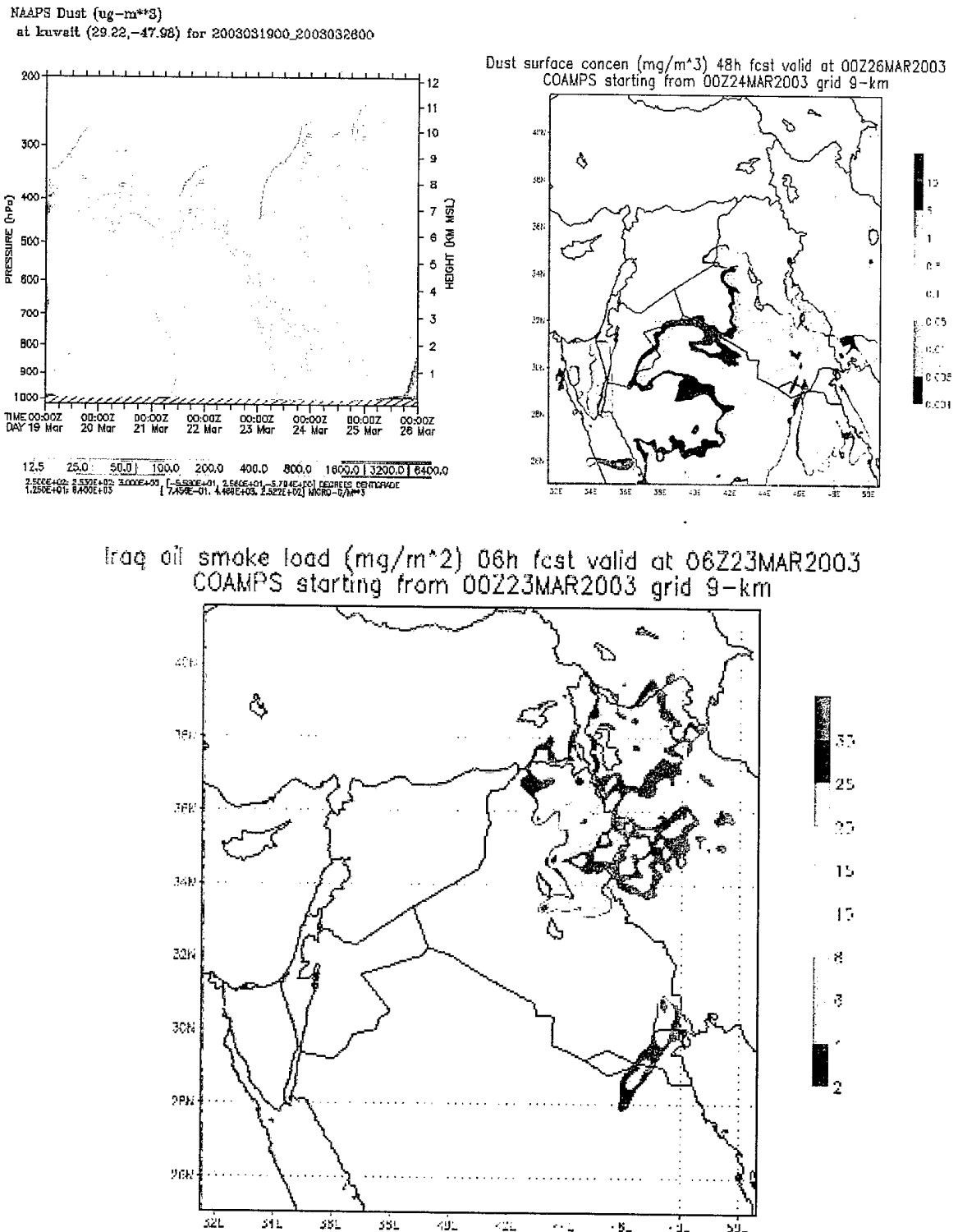COAMPS starting from 00Z23MAR2003 grid 9-km

Fig. 23 - Upper left, 5 day NAAPS cross-section of dust concentration for Kuwait, March 19-26, 2003. Upper right, COAMPS dust surface concentration for March 26, 2003. Lower, example image of oil fire smoke for March 23rd, 2003.

8. SUMMARY AND CONCLUSIONS

This report conveys the status and preliminary findings of the first year of work under the project "Evaluation of the Impacts of Aerosol Particles on High Energy Laser Performance by Using Community Data Sets and a Mesoscale Transport Model" funded by ONR Code 351. The rationale of this study was to determine an aerosol extinction climatology that would allow optimum wavelength selection for High Energy Laser systems deployed in the marine environment. As such systems would most likely be used in a coastal region, emphasis was placed on the Asian and Mediterranean environments.

Because of the overwhelming cost in performing field deployments to all of the relevant regions of the world to do an HEL assessment, it was decided that this study should focus on community data sets. For this purpose, this project would combine data from 5 sources: 1) Microphysical properties of aerosol particles would be gathered from the literature, 2) Ocean visibility reports would determine the frequency of severe visibility reducing events, 3) Remote sensing data would determine the temporal and spatial characteristics of clear sky events, 4) Near-surface models would be employed to specify extinction by sea salt near the ocean surface (where a naval HEL system would be used), and 5) An analysis of NAAPS data and specific propagation scenarios would be made using COAMPS™.

This project was intended to span 3 years, with the first year being devoted solely to data collection. However, preliminary analyses of parts of the data have already been completed and are presented here. Aerosol microphysics models considered "typical" for the world are presented with approximate wavelength dependence given for scattering and absorption. These models may reveal wavelengths at which scattering effects of aerosols are minimal. In particular, urban pollution and smoke have a relatively low impact in the near infrared, which implies that such wavelengths could be beneficial for operations in polluted coastal environments (such as east Asia, the Persian Gulf, and northern Mediterranean Sea). On the other hand, the water vapor absorption increases at lower wavelengths, and it is unclear at this stage which wavelengths in, say, the 1.06, 1.25, and 1.625 μm atmospheric window bands are optimal. The optimal choice depends on the relative contributions of water vapor, urban pollution and smoke, as well as the presence of dust and sea salt, which cause a relatively wavelength independent effect. Scintillation, which decreases with wavelength, is outside the scope of this study but should also be considered simultaneously. Consequently, a more thorough climatology is warranted.

Preliminary investigations of atmospheric visibility suggest that aerosol particles will contribute to light extinction in the near-IR in most strategic locations of the globe. For the analysis in this report, we use the 10-20 km and <10 km visibilities as key indicators, as 10 km is the likely engagement distance for a shipboard HEL system. For fine mode particles such as pollution and smoke, a 10 km visibility implies a ~50% reduction in energy over a path of 10 km at a wavelength of 1.06 μm. For the coarse mode, this would translate to ~85% reduction. Care must be taken in using these data, since we have found a significant bias between shore station and ship observation visibility (on the order of a factor of 2 to 8), with shore stations yielding lower values. The probability of visibility worse than 10 km falls off dramatically (e.g., visibility less than say 4 km is only <8% for all regions). Fair visibility can be expected over much of the Persian Gulf/Arabian Sea, the Mediterranean Sea, and coastal East Asia. In some sub-areas of these regions, three-month seasonal values (e.g., spring, summer, autumn, winter) can reach as high as 40-50% of days. At this time, it is unclear what are the relative effects of local pollution and data bias. Further study is clearly needed.

Remote sensing data ·was compiled from the AVHRR, TOMS, and MODIS platforms. Preliminary investigations show that while AVHRR and TOMS are good for estimating inter-annual ability of aerosol particle loadings in the atmosphere, the MODIS product is preferable for determining aerosol coverage and size. Coverage of significant aerosol events qualitatively matches visibility reports, with the most

impacted regions being the Persian Gulf, Arabian Sea, the North African Atlantic Coast, the Mediterranean Sea, and East Asian Seas. Further work is needed to develop a complete temporal characterization of these events.

Modeling work has taken two forms. First, near-surface studies were performed using the Advanced Navy Aerosol Model (ANAM) and the French-Dutch model SeaCluse. Previous estimates of aerosol extinction based on the Navy Aerosol Model (NAM) family of models which does not fully account for all possible aerosol species produces optimistic results when applied to coastal regions, and likely introduced an artifact wavelength dependence in light scattering in the near IR. ANAM provides better results for sea spray/spume for high wind conditions. Comparisons with the SeaCluse process model are underway and are necessary to understand the uncertainties in NAM-like regression models. The stage is also set for a climatology based on the global NRL Aerosol Analysis and Prediction System (NAAPS) and the mesoscale aerosol model imbedded in COAMPS™. Analysis based on the above models is necessary to unify the sometimes-conflicting datasets and allow this HEL analysis to move forward.

9. ACKNOWLEDGMENTS

REFERENCES

Andreas, E. L., A new sea spray generation function for wind speeds up to 32 m/s, *J. Phys. Oceanogr.*, 28, 2175-2184, 1998.

Andreas, E. L., J. B. Edson, E. C. Monahan, M. P. Rouault and S. D. Smith, The spray contribution to net evaporation from the sea: a review of recent progress, Boundary Layer Meteorol., 72., 3-52, 1995.

Ångstrom, A., On the atmospheric transmission of sun radiation and on dust in the air, Geogr. Ann., 12, 130-159, 1929.

Batten, L.J., Radar observation of the atmosphere, The University of Chicago, Chicago, pp. 324, 1973.

Benkovitz, C. M., T. Scholtz, L. Pacyna, L. Tarrson, J. Dignon, E. Voldner, P. A. Spiro, and T. E. Graedel, Global gridded inventories of anthropogenic emissions of sulphur and nitrogen. *J. Geophys. Res.*, 101, 29239-29253, 1996.

Beland, R. R., Propagation through atmospheric optical turbulence, in: The IR and EO systems Handbook, F. G. Smith (ed), Vol. 2, pp159-234, 1993.

Bergin M. H., G. R. Cass, J. Xu , C. Fang, L. M. Zeng, T. Yu , L. G. Salmon, C. S. Kiang, X. Y. Tang, Y. H. Zhang, and W. L. Chameides, Aerosol radiative, physical, and chemical properties in Beijing during June 1999, *J. Geophys. Res, 106*, 17969-17980, 2001.

Blanchard, D. C., A. H. Woodcock, and R. J. Cipriano, The veritcal distribution of the concentration of sea salt in the marine atmosphere near Hawaii, *Tellus*, 118-125, 1984.

Belcher, S. E., and J. C. R. Hunt, Turbulent flow over hills and waves, *Annu. Rev. Fluid. Mech., 30,* 507-538, 1998.

Brown, T., and A. K. Goroch, Climatology of surface infrared extinction coefficients in the North Atlantic ocean region, NAVENVPREDSCHFAC Technical Report, TR 82-04, August 1982.

Cachier, H., J. Ducret, M.-P. Bremond, V. Yoboue, J.-P. Lacaux, A. Gaudichet, and J. Baudet, Biomass Burning in a Savanah Region of the Ivory Coast, , in *Global Biomass Burning: Atmospheric, Climactic and Biospheric Implications*, edited by J. S. Levine, pp. 174-180, MIT Press, New York, 1991.

Christensen, J. H., The Danish eulerian hemispheric model - A three-dimensional air pollution model used for the Arctic. *Atmos. Env., 31*, 4169-4191, 1997.

Chu, D. A., J. Y. Kaufman, C. Ichoku et al. Validation of MODIS aerosol optical depth over land, *Geophys. Res. Lett.*, 29, MOD 1, 1-4, 2002.

Crutzen, P. J. and M.O. Andreae, Biomass burning in the tropics: Impact on atmospheric chemistry and biochemical cycles, Science, 250, 1669-1678, 1990.

D'Almeida, G. A., P. Koepke, and E. P. Shettle, Atmospheric aerosols, *in Global Climatology and Radiative Characteristics*, A. Deepak Publishing, Hampton, Virginia, USA, 1991.

DeLeeuw, G., Vertical profiles of giant particles close above the sea surface. *Tellus 38B*, 51-61, 1986a.

DeLeeuw, G., P. B. W. Schwering, P. J. Fritz and A. N. de Jong, Long-range IR propagation measurements over the North Sea. AGARD electromagnetic wave propagation panel 55th specialists' meeting on "Propagation assessment in coastal environments", Bremerhaven, Germany, 19-23 September, 1994. AGARD CP 567, paper 14 (published 1995).

DeLeeuw, G., A. M. J. van Eijk and D. R. Jensen, Marine Aerosol Properties and Thermal Imager Performance (MAPTIP): an overview, SPIE Proceedings 2828, 2-14, 1996.

Dubovik, O., B. N. Holben, T. F. Eck, A. Smirnov, Y. J. Kaufman, M. D. King, D. Tanre, I. Slutsker, 2002. Variability of absorption and optical properties of key aerosol types observed in worldwide locations, *J. Atmos. Sci, 59*, 590-608.

Exton, H. J., J. Latham, P. M. Park, M. H. Smith, and R. R. Allan, The production and dispersal of maritime aerosol, In *Oceanic Whitecaps and their Role in Air-Sea exchange Processes*. E. C Monahan and G. Mac Niocaill eds., pp. 175-193, D. Reidel, Norwell, Mass., 1986.

Fairall, C. W., K. L. Davidson and G. E. Schacher, Meteorological models for optical properties in the marine atmospheric boundary layer. *Opt. Eng. 21*, 847-857, 1982.

Fairall, C. W., K. L. Davidson, and G. E. Schacher, An analysis of the surface production of sea-salt aerosols, *Tellus, 35B*, 31-39, 1983.

Fitzgerald, J. M., Marine Aerosols: a review. *Atmos. Environ.* **25A**, 533-545, 1991.

Ganor, E., H. A. Foner, S. Brenner, E. Neeman, and N. Lavi, The chemical composition of aerosols settling in Israel following dust storms, *Atmos. Environ.* **25**, 2665-2670, 1991.

Gao, Y., and J. R. Anderson, Characteristics of Chinese aerosols determined by individual-particle analysis, *J. Geophys. Res., 106*, 18,037-18,045, 2001.

Gathman, S. G., Optical Properties of the Marine Aerosol as Predicted by the Navy Aerosol Model, *Opt. Engin., 22*, 57-62, 1983.

Gathman, S. G., A preliminary description of NOVAM, the Navy Oceanic Vertical Aerosol Model, NRL report 9200, NRL Washinton DC, 1989.

Gathman, S. G., A. M. J. van Eijk and L. H. Cohen, Characterizing large aerosols in the lowest levels of the marine atmosphere, *SPIE Proceedings 3433*, 41-52, 1998.

Gaudichet, A., F. Echalar, B. Chatenet, J. P. Quisefit, G. Malingre, H. Cachier, P. Buat-Menard, W. Maenhaut, Trace Elements in Tropical African Savanna Biomass Burning Aerosols, *J. Atmos. Chem., 22*, 19-39, 1995.

Geogdzhayev, I., M. Mishchenko, W. Rossow, B. Cairns, A. Lacis, Global two-channel AVHRR retrievals of aerosol properties over the ocean for the period of NOAA-9 observations and preliminary retrievals using NOAA-7 and NOAA-11 Data, *J. Atmos. Sci., 59*, 262-278, 2002.

Gerber, H., Relative Humidity Parameterization of the Navy Aerosol Model (NAM), NRL Report 8956, December 30, 1985.

Gomes, L., G. Bergametti, G. Coude-Gaussen, and P. Rognon, Submicron desert dusts: a sandblasting process, *J. Geophys. Res., 95*, 13,927-13,935, 1990.

Gomes, L., and D. A. Gillette, A comparison of characteristics of aerosol from dust storms in central Asia with soil derived dust from other regions, *Atmos. Environ.* **27A**, 2539-2544, 1993.

Goroch, A. K., and T. Brown, Frequency of adverse weather conditions affecting high energy laser systems operations, NAVENVPREDRSCHFAC Technical Report TR 80-06, November 1980.

Griffing, G. W.,. Relations between the prevailing visibility, nephelometer scattering coefficient and sun photometer turbidity coefficient. Atmospheric Environment 14, 577-584, 1980.

Hartley, W. S., P. V. Hobbs, J. L. Ross, P. R. Russell, J. M. Livingston, "Properties of aerosols aloft relevant to direct radiative forcing off the mid-Atlantic coast of the United States," *J. Geophys. Res.* **105**, 9859-9885, 2000.

Hegg, D.A., J. Livingston, P.V. Hobbs, T. Novakov, and P. Russell, Chemical apportionment of aerosol column optical depth off the mid-Atlantic coast of the United States, *J. Geophys. Res., 102*, 2213-2222, 1997.

Herman, J. R., P. K. Bhartia, O. Torres, N. C. Hsu, C. J. Seftor, and E. Celarier, Global distribution of UV-absorbing aerosols from Nimbus-7/TOMS data, J. Geophys. Res., 102, 16,911-16,922, 1997.

Hobbs, P. V., J. S. Reid, R. A. Kotchenruther, R. J. Ferek, R. Weiss, 1997. Direct radiative forcing by smoke from biomass burning, Science, 275, 1776-1778.

Hogan, T. F., and T. E. Rosmond, The description of the Navy operational global atmospheric prediction system's spectral forecast model. *Mon. Wea. Rev., 119*, 1786-1815, 1991.

Hogan, T. F., and L. R. Brody, Sensitivity studies of the Navy's global forecast model parameterizations and evaluation of improvements to NOGAPS. *Mon. Wea. Rev.,121,* 2373-2395, 1991.

Hoppel, W., J. W. Fitzgerald, G. M. Frick, R. E. Larson, and E. J. Mack, Atmospheric aerosol size distributions and optical properties found in the marine boundary layer over the Atlantic Ocean, NRL Report 9188, Naval Research Laboratory, Washington, DC, 75 pp. [NTIS AD-A210800], 1989.

Hughes, H. G., Evaluation of the LOWTRAN6 Navy maritime aerosol model using 8 to 12 μm sky radiances. *Opt. Eng. 26,* 1155-1160, 1987.

Hsu, N. C., J. R. Herman, P. K. Bhartia, C. J. Seftor et al. Detection of biomass burning smoke from TOMS measurements, *Geophys. Res., Lett.,* 23, 745-748, 1996.

Hufnagel, R. F., Propagation through atmospheric turbulence, in: The infrared handbook. W. L. Wolfe and G. J. Zissis (eds), Environmental Research Institute of Michigan, 1978.

Husar R. B., J. D. Husar, and L. Martin, Distribution of continental surface aerosol extinction based on visual range data. Atmos. Environ, 34,5067-5078 2000.

Intergovernmental Panel on Climate Change (IPCC). *Climate Change 1994: Radiative Forcing of Climate Change,* edited by J. T. Houghton et al. Cambridge Univ. Press, Cambridge, 1995.

Intergovernmental Panel on Climate Change (IPCC), *Climate Change 2001: The scientific basis,* edited by J. T. Houghton et al. Cambridge Univ. Press, Cambridge, 2001.

John, W., S. M. Wall, J. L. Ondo, and W. Winklmayr, Modes in the size distribution of atmospheric inorganic aerosols, Atmos. Environ., 24A, 2349-2359, 1990.

Kaufman Y. J., D. Tanre, O. Dubovik, A. Karnieli, L. A. Remer, Absorption of sunlight by dust as inferred from satellite and ground-based remote sensing, Geophys. Res. Lett , 28, 1479-1482, 2001.

Kotchenruther, R. A., and P. V. Hobbs, Humidification factors of aerosols from biomass burning in Brazil, *J. Geophys. Res., 103,* 32,081-32,090, 1998.

Kotchenruther, R. A., P. V. Hobbs, D. A. Hegg, Humidification factors for atmospheric aerosols off the mid-Atlantic coast of the United States, *J. Geophys. Res., 104,* 2239-2251, 1999.

Kravtsov, Y. A. and Orlov, Y. I., Geometrical optics of inhomogeneous media, Springer , Berlin, 1990.

Le Canut. P., M. O. Andreae, G. W. Harris, F. G. Wienhold, and T. Zenker, Aerosol optical properties over southern Africa during SAFARI-92, in Biomass Burning and Global Change, edited by J. S. Levine, pp. 441-459, MIT Press, Cambridge, Mass., 1997.

Li-J X, H. B. Maring, J. M. Prospero, Effect of relative humidity on light scattering by mineral dust aerosol as measured in the marine boundary layer over the tropical Atlantic Ocean, J. Geophys. Res., 103, 31,113-31,121, 1998.

Liousse, C., C. Devaux, F. Dulac, H. Cachier, Aging of savannah biomass burning aerosols: Consequences on their optical properties, *J. Atmos. Chem., 22,* 1-17, 1995.

Martins, J. V., P. Artaxo, P. V. Hobbs, C. Liousse, H. Cachier, Y. Kaufman, and A. Plana-Fattori, Particle size distributions, elemental compositions, carbon measurements, and optical properties of smoke from biomass burning in the Pacific Northwest of the United States, In *Global Biomass Burning and Global Change.* ed. J. S. Levine, MIT Press, Cambridge, Mass, pp 716-732, 1996.

McCartney, E. J., Optics of the atmosphere: scattering by molecules and particles, John Wiley and Sons, New York, 1976.

Mestayer, P. G., A. M. J. van Eijk, G. de Leeuw and B. Tranchant, Numerical simulation of the dynamics of sea spray over the waves.. J. Geophys. Res. 101, 20771-20797, 1996.

Miles, J. W., On the generation of surface waves by shear flow, *J. Fluid Mech., 3,* 185-204, 1957.

Navarro, L. J., A. M. J. van Eijk and P. G. Mestayer, Impact of the eddy diffusivity on the vertical aerosol concentration. *J. Aerosol Sci. 32,* S1089-1090, 2001.

Novakov, T., 1982. Soot in the atmosphere, in *Particulate carbon: Atmospheric life cycle,* edited by G. T. Wolf and R. L. Klimish, pp. 19-41, Plenum, New York.

Panofsky, H. A. and J. A. Dutton, Atmospheric turbulence, John Wiley New York, 1984.

Patterson, E. M., Optical properties of the crustal aerosol: Relation to chemical and physical characteristics, *J. Geophys. Res., 86,* 3236-3246, 1981.

Patterson, E. M., and D. A. Gillette, Commonalities in measured size distribution for aerosol having a soil-derived component, *J. Geophys. Res., 82,* 2074-2082, 1977.

Pernter, J. M. and Exner, F. M., Meteorologische Optik, Wilhelm Braumueller, Univesitaets-Verlagsbuchhandlung, Wien/Leipzig, pp. 907, 1922.

Porter, J., and A. D. Clarke, Aerosol size distribution models based on in situ measurements, *J. Geophys. Res.,102*, 6035-6045,1997.

Prins, E. M., J. M. Feltz, W. P. Menzel, and D. E. Ward, An overview of GOES 8 diurnal fire and smoke results for SCAR-B and the 1995 fire season in South America, *J. Geophys. Res., 103,* 31,821-31,836, 1998.

Radke L.F., D.A. Hegg, P.V. Hobbs, J.D. Nance, J.H. Lyons, K.K. Laursen, R.E. Weiss, P.J. Riggan, and D.E. Ward. Particulate and trace emissions from large biomass fires in North America, in Global Biomass Burning: Atmospheric, Climatic, and Biospheric Implications, edited by J. S. Levine, pp. 209-224, MIT Press, Cambridge, MA., 1991.

Reid J. S., T. A. Cahill, and M. R. Dunlap, Geometric/aerodynamic size ratios of ash aggregates from burning Kuwaiti oil fields, *Atmos. Environ., 28,* 2227-2234, 1994

Reid J. S., R. G. Flocchini, T. A. Cahill, R. S. Ruth, and D. P. Salgado, Local meteorological, transport, and source aerosol characteristics of late Autumn Owens Lake (dry) dust storms, *Atmos. Environ., 28,* 1699-1706, 1994.

Reid, J. S., and P. V. Hobbs, Physical and optical properties of smoke from individual biomass fires in Brazil, *J. Geophys. Res., 103,* 32,013-32,031, 1998.

Reid, J. S., H. H. Jonsson, M. H. Smith, and A. Smirnov, Evolution of the vertical profile and flux of large sea-salt particles in a coastal zone, *J. Geophys. Res., 106,* 12,039-12,053, 2001.

Reid, J. S., H. H. Jonsson, H. B. Maring, A. A. Smirnov, D. L. Savoie, S. S. Cliff, E. A. Reid, M. M. Meier, O. Dubovik, and S-C Tsay, Comparison of Size and Morphological Measurements of Coarse Mode Dust Particles from Africa, *J. Geophys. Res.,* in press, 2003.

Remer, L. A., J. Y. Kaufman, et al. Validation of MODIS aerosol optical depth over ocean, *Geophys. Res., Lett.,* in press, 2002.

Robock, A., 1991. Surface Cooling due to forest fire smoke, *J. Geophys. Res., 96,* 20,869-20,878.

Schwering, P. B. W., Atmospheric effects on FPA's in IRST's, *SPIE Proceedings 2552,* 247-258, 1995.

Shettle, E. P., and R. W. Fenn, Models for the aerosols of the lower atmosphere and the effects of humidity variations on their optical properties, AFGL-TR-79-0214, 94 pp, 1979.

Skolnik, M. I., Introduction to radar systems, McGraw-Hill, New York, pp. 506-511, 1962.

Sokolik, I. N., and O. B. Toon, Incorporation of mineralogical composition into models of the radiaitve properties of mineral aerosols from UV to IR wavelengths, *J. Geophys. Res., 104,* 9423-9444, 1999.

Stowe, L., A. Ignatov, and R. Singh, Development, validation, and potential enhancements to the second-generation operational aerosol product at the National Environmental Satellite, Data and Information Service of the National Oceanic and Atmospheric Administration, J. Geophys. Res., 102, 16,923-16,934, 1997.

Tanre, D., P. Y. Deschamps, C. Devaux, M. Herman, Estimation of Saharan aerosol optical thickness from blurring effects in thematic mapper data, J. Geophys. Res., 93, 15955-15964, 1988.

Thomas, M. E. and D. D. Duncan, Atmospheric transmission, in: The IR and EO systems Handbook, F. G. Smith (ed), Vol. 2, pp 1-158, 1993.

Tomasi, C., E. Caroli, V. Titale, Study of the relationship between Ångstrom's wavelength exponent and Junge particle size distribution exponent, J. Climate Appl. Meteor., 22, 1707-1716, 1983.

Torres, O., P. K. Bhartia, J. R. Herman, Z. Ahmad, and J. Gleason, Derivation of aerosol properties from satellite measurements of backscattered ultraviolet radiation, Theoretical basis, J. Geophys. Res., 103, 17,099-17,100, 1998.

Van Eijk, A. M. J., B. J. S. Tranchant and P. G. Mestayer, SeaCluse : numerical simulation of evaporating sea spray droplets, *J. Geophys. Res. 106,* 2573-2588, 2001.

Van Eijk, A. M. J., L. H. Cohen, L. J. Navarro and G. DeLeeuw, Near-surface aerosol transmission in the marine environment, *SPIE Proceedings 4884,* 160-169, 2002.

Wall, S.M., W. John, and J.L. Ondo, "Measurements of Aerosol Size Distributions for Nitrate and Major Ionic Species," Atmos. Environ. 22, 1649-1656, 1988.

Weiss, R.E. and P.V. Hobbs, "Optical Extinction Properties of Smoke from the Kuwait Oil Fires," J. Geophys. Res. **97**, 14,537-14,540, 1992.

Westphal, D. L., O. B. Toon, Simulations of microscale, radiative, and dynamical processes in a continental-scale forest fire smoke plume, J. Geophys. Res., 96, 22,379-22,400, 1991.

Westphal, D.L., O.B. Toon, and T.N. Carlson, "A Case Study of Mobilization and Transport of Saharan Dust," *J. Atmos. Sci.* **45**, 2145-2175, 1988.

Whitby, K.T., "The Physical Characteristics of Sulfur Aerosols," *Atmos. Environ.* **12**, 135-155, 1978.

Woods, D.C., R. L. Chuan, W. R. Coffer III, J. S. Levine, 1991. Aerosol characterization in smoke plumes from a wetlands fire, in Global Biomass Burning: Atmospheric, Climactic and Biospheric Implications, edited by J. S. Levine, pp. 240-244, MIT Press, New York.

Wu, J., "Evaporation Due to Spray," *J. Geophys. Res.* **79**, 4107-4109, 1974.

Zuev, V.E., *Propagation of Visible and Infrared Radiation in the Atmosphere* (John Wiley and Sons, New York, 1974).

APPENDIX A. PROJECT TEAM

PI: **Dr. Jeffrey S. Reid**, Code 7534 Aerosol and Radiation Modeling Section, Marine Meteorology Division, Naval Research Laboratory, 7 Grace Hopper St., Stop 2, Monterey, CA 93943-5502
Email: reidj@nrlmry.navy. mil, Phone: (831) 656-4725, Fax: (619) 656-4769

Co-PI and Technical Oversight: **Mr. Joung Cook**, Naval Research Laboratory Code 6335, 4555 Overlook Avenue, SW, Washington, DC 20375-5200;
E-Mail: Joung.Cook@nrl.navy.mil, Phone: (202) 767-2319, Fax (202) 767-6980

Co-PI: **Dr. Si Chee Tsay**, Climate and Radiation Branch Code 913, NASA Goddard SFC, Greenbelt MD, 20771.
Email: Tsay@climate. gsfc. nasa. gov, Phone: (301) 614-6188, Fax: (301) 614-6307

Co-PI: **Dr. Alexander VanEijk**, TNO Physics and Electronics Laboratory, P. O. Box 96864, 2509 JG The Hague, The Netherlands
Email: vanEijk@sel. tno. nl Phone: + 31 70 374 0451, Fax: + 31 70 374 0654

Co-PI: **Dr. Douglas L. Westphal**, Code 7534 Aerosol and Radiation Modeling Section, Marine Meteorology Division, Naval Research Laboratory, 7 Grace Hopper St., Stop 2, Monterey, CA 93943-5502
Email: westphal@nrlmry. navy. mil, Phone: (831) 656-4743, Fax: (619) 656-4769

Co-Investigators :

Allen Chu, University of Maryland, Baltimore County, GEST Center

R.J. Decae, TNO Netherlands

Ming Liu, Naval Research Laboratory, Marine Meteorology Division

William Moision, SPAWAR Systems Center, San Diego, Code 858

Richard Paulus, SPAWAR Systems Center, San Diego, Code 858

APPENDIX B. LIST OF ACRONYMS

AMP	Air Mass Parameter
AMSL	Above Mean Sea Level
ANAM	Advanced Navy Aerosol Model
ASTD	Air-Sea Temperature Difference
CAM	Coastal Aerosol Model
CIRPAS	Center for Interdisciplinary Remotely Piloted Aircraft Studies
CLUSE	Couche Limite Unidimensionelle Stationnaire d'Embruns
COAMPS™	Coupled Ocean/Atmosphere Prediction System
EO	Electro-optical
EOPACE	Electro-optical Propagation Assessment in the Coastal Environment
EOSTAR	Electro-Optical System Transmission and Ranging
EOTDA	Electro-Optical Tactical Decision Aid
FLIP	Floating Instrument Platform
FLIR Sensor	Forward Looking Infrared Sensor
FNMOC	Fleet Numerical Meteorology Oceanography Center
FPN	Forschungsplatform Nordsee
FSSP	Forward Scattering Spectrometer Probe
GOES	Geostationary Observing Environmental Satellite
GSFC	Goddard Space Flight Center
HEL	High Energy Laser
IR	Infrared
IRST	Infrared Search and Track
IRTSS	IR Target-Scene Simulation Software
JIATF	Joint Interagency Task Force
LOWTRAN	Low Resolution Transmission
LR-IRST	Long Range Infra Red Search and Track
LWIR	Long Wave IR
MAPTIP	Marine Aerosol Properties and Thermal Imager Performance
MBL	Marine Boundary Layer
MDR	Maximum Detection Range
MODTRAN	Moderate resolution Transmission code
MPN	MeetPost Noordwijk
MuSES	Multi-Service Electro-optic Signature (target radiance prediction code)
MWIR	Mid Wave IR
NAAPS	NRL Aerosol Analysis and Prediction System
NAM	Navy Aerosol Model
NASA	National Aeronautics and Space Administration
NOGAPS	Navy Operational Global Atmospheric Prediction System
NOVAM	Navy Oceanic Vertical Aerosol Model
OAP	Optical Array Probe
ONDCP	Office of National Drug Control Policy
PCASP	Passive Cavity Aerosol Spectrometer Probe
R/P	Research Platform
RED	Rough Evaporation Duct experiment
SeaPlus	Sea (radiance) Plus (clutter prediction code)

SeaRad	Sea Radiance (prediction code)
TAWS	Target Acquisition Weather Software
TEDS	Tactical Environmental Database System
TNO	Netherlands Organisation for Applied Scientific Research
TNO-FEL	TNO Physics and Electronics Laboratory
WAMPS	Weather Automated Mission Planning Software